Electrical Discharge Interaction with Lithium-Ion Battery Vent Gases

Investigations using High-Speed Imaging and Breakdown Analysis

Alexander Petersson

LUNDS UNIVERSITET

Department of Energy Sciences, Faculty of Engineering

Msc Thesis
ISRN LUTFD2/TFRT--9999--SE
ISSN 0280-5316

Department of Energy Sciences, Lund University
Lund University
Box 118
SE-221 00 LUND
Sweden

Printed in Sweden by Media-Tryck
Lund 2023

Abstract

The increasing drive for sustainable and eco-friendly transportation has made the electrification of cars a top priority in the energy and transportation sectors. Ensuring the safety of electrical vehicle (EV) batteries is of the utmost importance. This collaborative research project, conducted in partnership with Volvo Cars, focuses on optimizing battery safety by investigating the risks associated with battery fires.

This study focuses primarily on lithium-ion batteries and explores the possibility of electrical discharge within them, as well as ignition behaviors resulting from thermal runaway. By examining the combination of electrical discharge and combustible gases, the project delves into the uncertainties surrounding electrical discharge as an ignition source in abused batteries to gain insights into associated risks and possible preventative design.

Through the use of high-speed imaging and laser diagnostics, two experiments were performed to assess this interaction. With one experiment focusing on electrical discharge through different gas media, and the other focusing on the behavior of the combustion of ignited vent gases, many significant aspects are investigated and analyzed. The outcomes of this study provide valuable insight for enhancing battery safety, and create a stepping stone into this relatively unstudied field.

Keywords:
Electrical Discharge, Electrical Arc, Spark Discharge, Combustion, Ignition, Lithium-Ion Battery, Thermal Runaway, Vent Gases, Breakdown Voltage, Ionization, High-Speed Imaging

Acknowledgements

I would like to express my deepest appreciation to Volvo Cars and the Department of Physics at Lund University for their invaluable contributions to the development and execution of this research. Their support, expertise and guidance have played a critical role in the completion of this thesis work.

First, I want to extend my deepest appreciation to Arman Subash, my lab supervisor, for the enormous part he has played throughout this project. The daily guidance, advice, knowledge, and light-hearted environment he created in the laboratory and in the department made the entire duration of this project an incredibly enjoyable experience.

I would also like to extend my sincere gratitude to Elna Nilsson, my thesis supervisor, for her major contributions to this work. Her unwavering guidance, enthusiasm, and expertise added considerably to this thesis experience.

I would also like to acknowledge and thank Julia Lövgren, my colleague throughout this research project. It was a pleasure working with her on this project, and she played a large part in making this journey a successful and enjoyable experience.

Finally, I would like to thank Andreas Ehn, Sebastian Nilsson, Yupan Bao, and Christian Brackmann for their continued support and guidance, along with the rest of the students, professors, and researchers at the Department of Combustion Physics for creating a pleasant and welcoming environment.

Contents

1. Introduction

1.1 Project Motivation

Due to the increasing motivation for sustainable and clean transportation, the electrification of cars has become a top priority in the energy and transportation sectors. As the prevalence of batteries continues to increase, safety becomes more important than ever. The work done in the scope of thesis research is performed in collaboration with Volvo Cars and focuses on optimizing battery safety in regards to electric vehicle battery fires. This project is in a relatively new field of study, as it addresses an issue that becomes more relevant as the transition to low emission transportation begins to grow. This provides an exciting opportunity to work in collaboration with one of the top car manufacturers in the world to improve safety.

The most common kind of battery used in electrical vehicles today is the lithium-ion battery. As research and designs in the electrification of vehicles continue to improve, the voltage of these car batteries has increased in magnitude. For example, manufacturers today are aiming to be able to have 800 or 1000 V battery systems powering their vehicles, in comparison to the 300 V battery system used in the first widely commercialized electric vehicles. This increased voltage provides better range and charging time and has been made possible with the introduction of more aggressive battery chemistries.

As batteries undergo abuse from overuse, overcharging, excessive heating, mechanical wear, or otherwise, the possibility for thermal runaway becomes more prevalent. Thermal runaway is an event in which a chain of chemical reactions produce heat in such a way that prohibits sufficient heat dissipation within the battery, leading to an uncontrolled temperature increase [2]. This thermal runaway can cause a leakage of vent gases within the battery enclosure. Depending on the battery chemistry, these gases can be combustible, and in combination with the possibility of electrical discharge, may present a threat for ignition. Although this is a rare occurrence, safety measures must be taken to reduce the risk of this happening.

The combination of electrical discharge introduces an interesting combination. Much is known across industry and academic fields regarding ignition and combustion, and much is known about electrical discharge, gas ionization and plasma as separate topics. However, when you combine the two, there is an aura of uncertainty surrounding electrical discharge as the **source** of ignition in a combustible gas mixture.

Additionally, once these combustible gases have been ignited, it is important to understand the combustion behavior and the and the behavior of the flame. Previous research and experiments performed at Lund University's Department of Combustion Physics have found the possible combination of gases to exhibit a number of different behaviors. Understanding how the flame will behave once combustion occurs, and why it behaves this way, provides a critical insight into the level of risk associated with this combustion. The aforementioned motivation for this project is derived from this risk. The research questions and methodology derived from the need to maximize battery safety will be described in the following sections.

1.2 Project Foundation and Execution

This project was carried out in collaboration with Volvo Cars in Gothenburg, Sweden with the main contacts Ivan Rexed and Leopold Werberg. Additionally, it will be performed under the supervision of Elna Nilsson and Arman Subash in the Department of Combustion Physics of LTH in Lund, Sweden. Additional collaboration with other members of academia (from LTH) were utilized, and have been approved by Volvo Cars. All professors and researchers have been credited and cited, and were instrumental throughout the entirety of this work.

The work done in the scope of this master's thesis was performed in tandem with another master's student of LTH, Julia Lövgren. The scope of her experiment slightly differed in the second experiment. Whereas this report uses high-speed imaging to identify trends in the ignition event and flame behavior, Lövgren's work, "Discharge and Flame Chemistry in Lithium-Ion Battery Vent Gases Investigations using Breakdown Experiments with Laser-Based Diagnostics" utilized laser diagnostics, specifically OH-PLIF, to identify flame chemistries across the same test cases. Results from Lövgren's OH-PLIF findings will be briefly mentioned to support conclusions drawn from the high-speed imaging research, but for in-depth analysis of Lövgren's OH-PLIF results, please see [5].

The setup of the laboratory, safety documentation, experimental methodology and execution of the experiments were done in collaboration with Lövgren. The experiments were performed simultaneously, while different pieces of equipment (high-speed camera and laser diagnostics computer) were controlled by Petersson and Lövgren, respectively. The experiments were designed, set up and executed together under the supervision of Arman Subash.

An addendum can be found in the Appendix providing a detailed description of the overall experimental setup.

1.3 Objectives and Research Questions

This master's thesis project will focus on the experimental and theoretical phenomena taking place in the ignition of combustible battery vent gases resulting from electrical discharge. It will be carried out in conjunction with Volvo Cars using data provided by them, experimental data collected in the labs of LTH's Department of Combustion Physics, and a number of literature (and personal/ professional) resources in the related academic fields.

The current goal of this project is two-fold: To investigate the prerequisites for formation of electrical discharge in relevant gas mixtures *and* to investigate the ignition event and flame behavior as a result of ignition from electrical discharge. The two gas mixtures that will be analyzed were chosen to be representative of common battery chemistries known as Lithium Nickel-Cobalt Aluminum Oxide (NCA) and Lithium Iron Phosphate (LFP) batteries. In addition to being two popular battery chemistries, these gases have also been shown to be on the highly explosive end (NCA) and less explosive end (LFP) of the spectrum as far as common battery vent gas mixtures are concerned [3]. The analysis of both ends of this spectrum makes it possible to identify trends that are strongly dependent on certain gas flow parameters and provide a strong foundation for further research in this area.

The following subsections show the focus areas and their respective research questions.

Electrical Discharge Frequency

The electrical discharge occurring in the electrical vehicles is not a well understood phenomenon. It happens at inconsistent intervals and locations in the battery modules when heat is intentionally introduced during testing, demonstrating a necessity of research in this area. Different environments affect the likelihood of an electrical discharge to form. Considering this, it is important to understand the minimum breakdown voltage of different gases (detailed in section 3.1), and how this can be related back to the project specific case in order to understand the risk of an electrical discharge.

Building upon Arman Subash's experimental setup from the pre-study conducted in 2022 titled "Electrical arcing as an ignition source in malfunctioning batteries," tests were designed to identify trends while varying a number of parameters. The minimum breakdown voltage was recorded for various gas mixtures, temperatures, distances and gas flow rates in order to identify trends that can create a foundation for better understanding of electrical discharge across a multitude of environments. The electrical discharge experiment, to be explained in detail in Chapter 3, aims to answer the following research questions:

> How do different gas media factor into the breakdown voltage at which electrical discharges occur?
>
> How do gas flow velocity and gas temperature affect the breakdown voltage?
>
> How does electrode separation distance affect the breakdown voltage?

Ignition and Flame Behavior

Performed in a separate experiment, high speed imaging will be used to capture the behavior of the flame after ignition. This will be done for 2 different gas mixtures, chosen to be representative of the highest and lowest explosive mixtures of the battery vent gases. The captured images will be used to analyze parameters and behaviors that can be useful in predicting the flame environment, such as equivalence ratio, emissive species and pre-mixing level of the fuel/air combination. Other properties, such as combustion rate and reaction path will also be examined.

As it was mentioned previously, Julia Lövgren's involvement in this experiment focused on using laser diagnostics to identify flame chemistry trends. High-speed images and OH-PLIF images were recorded for the same test cases, so that they may be used to analyze the same flame in a different manner.

This experiment closely follows the methodology set forth in Subash's pre-study, with some variations implemented to provide additional information. This experiment, explained in-depth in Chapter 4, aims to answer the following research questions:

What is the time scale of the ignition event?

How do different parameters affect the flame behavior and intensity?

What drives the combustion of the battery vent gases when exposed to electrical discharge?

1.4 Thesis Report Format

The research and experimental work performed in the scope of this thesis work included two types of experiments, both of which involved many theoretical concepts across different fields. These experiments, and the results obtained from them, were built on the pre-study by Arman Subash. In this pre-study, certain trends and phenomena were identified that require further investigation to increase understanding. For the sake of organization, a separate chapter summarizing the pre-study experimental setup and results will immediately follow Chapter 1. Next, these two experiments will be presented in separate chapters. The chapters will include relevant background knowledge, methodology, experimental setup, results and discussion for the respective experiment. This will be followed by a chapter discussing future outlook in both industry and academia as it pertains to topics discussed in this report. Finally, the conclusion chapter will summarize the work done throughout the span of this thesis work.

2. Pre-Study: A Need for Further Investigation

This chapter will provide a summarization of the work completed by Arman Subash supervised by Elna Nilsson in the pre-study “Electrical arcing as a source of ignition in malfunctioning batteries,” [4]. It is necessary to dedicate a chapter to this pre-study as it provides a better understanding of where the pre-study left off, and where the scope of the thesis research performed and explained in this report begins. Much of the experimental setup utilized in the pre-study stayed the same, but there were many changes and adaptations made to the setup to accommodate slightly different experimental objectives. In order to understand the whole picture of the work performed for this thesis work, it is necessary to mention the foundation provided by this pre-study. For further insight into the development of this work, refer to the pre-study itself. The relevant background knowledge for this experiment will be mentioned in Chapters 3 and 4, as they apply to their respective experiments. The purpose of this chapter is to simply provide an understanding for the reader as to the starting point of the thesis work.

2.1 Pre-study Introduction and Objectives

In 2022, Arman Subash of the Department of Combustion Physics of Lund University, in collaboration with project supervisor Elna Nilsson performed a pre-study involving the analysis of the combustion of battery vent gases. This project was funded by the Swedish Electromobility Centre, as well as other academic and industry partners. This pre-study served as a basis for all of the thesis work produced in this report. Results gathered in the pre-study were used to select certain criteria in the experiments detailed in sections Chapter 4, and almost all equipment used in the pre-study experiments were utilized in some capacity for the subsequent thesis research experiments.

The motivation for this pre-study is similar to the motivation of this thesis work, laid out in Section 1.1. Two battery chemistries were selected to be representative of a relatively highly explosive battery vent gas (NCA) and a low explosive vent gas (LFP). Table 2.1 shows the compositions of these gas mixtures. These two gases were selected based on a study performed by this project’s supervisor, Elna Nilsson, seen in [3] in which it mentions the popularity of these two battery chemistries. Using high-speed imaging at 10kHz, flame behavior was recorded and analyzed for an equivalence ratio range from 0.9-5, with gas flow rates of 5, 10 and 15 m/s, and gas temperatures of 200, 300 and 400 C.

Gas Mixtures	CO_2	CO	H_2	CH_4	C_2H_4	C_2H_6
NCA	10	37.1	42.8	7.1	3	0
LFP	48.4	9	29.5	5.6	7	0.5

Table 2.1: Gas compositions of analyzed battery vent gases

As these gas mixtures are unlikely to auto-ignite at atmospheric pressure, there must be an external ignition source for these gases to pose a safety threat. In and around the electrical vehicle battery systems, electrical discharge can pose that threat. As it has been mentioned multiple times, and is clearly the overall motivation for this research, gaining an in-depth understanding of the interaction of electrical discharge and combustible battery vent gases is instrumental in maximizing safety in electrical vehicles today. Background knowledge and a literature review summarizing research done in similar fields will be found in Chapters 3 and 4.

2.2 Pre-study Experimental Setup

This section will discuss the experimental setup of the lab work performed in the pre-study. This is significant in understanding the improvements and changes made to the setup in the scope of this master's thesis work. The improved experimental setup will be explained in detail in Chapters 3 and 4.

The three main aspects of the pre-study experimental setup can be divided into three parts: gas supply, power supply, and discharge setup.

Gas Supply

The configuration of the gas supply was designed such that an inert gas has the ability to be routed through a heating furnace, then flow into a tee and mix with two other gas flows. One of these other gas flows is pure Oxygen, O_2. The third gas flow consisted of the gas chosen to be representative of the battery vent gases in two separate cases. A description of these gases and justification of their representation can be found in Section 2.1. The figure below provides a visual schematic of the three-line configuration used in the pre-study. This configuration was not adjusted for the experiments performed for the thesis research.

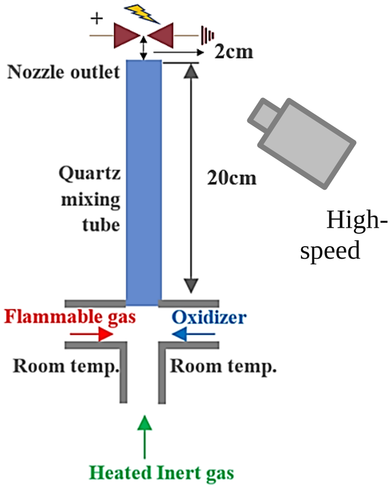

Figure 2.1: Gas flow configuration and experimental setup from [4]

Power Supply

The power supply connected to the electrodes was capable of delivering up to 16 kV at 500A. It consisted of a capacitor charger connected to a capacitor bank. The charging module provided a set current to the capacitor bank until a specific voltage was reached. At this point, electrical discharge would occur between the electrodes, and the capacitor bank would lose charge.

For safety reasons, a number of grounding wires were implemented to minimize the possibility of exposing oneself to lingering current. A high voltage, well-insulated wire ran from the power supply to the anode. Another wire was connected from the cathode to the ground of the power supply. There were some slight improvements to the grounding wiring made in the thesis research, but the power supply remained exactly the same.

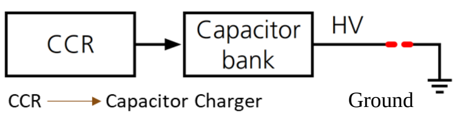

Figure 2.2: Power Supply Configuration from [4]

Electrode Setup

The electrode setup in the pre-study was made up of a block of Teflon cut into a "U" shape, with the electrodes laying in a horizontal orientation above the quartz tube. The setup can be seen in the images below:

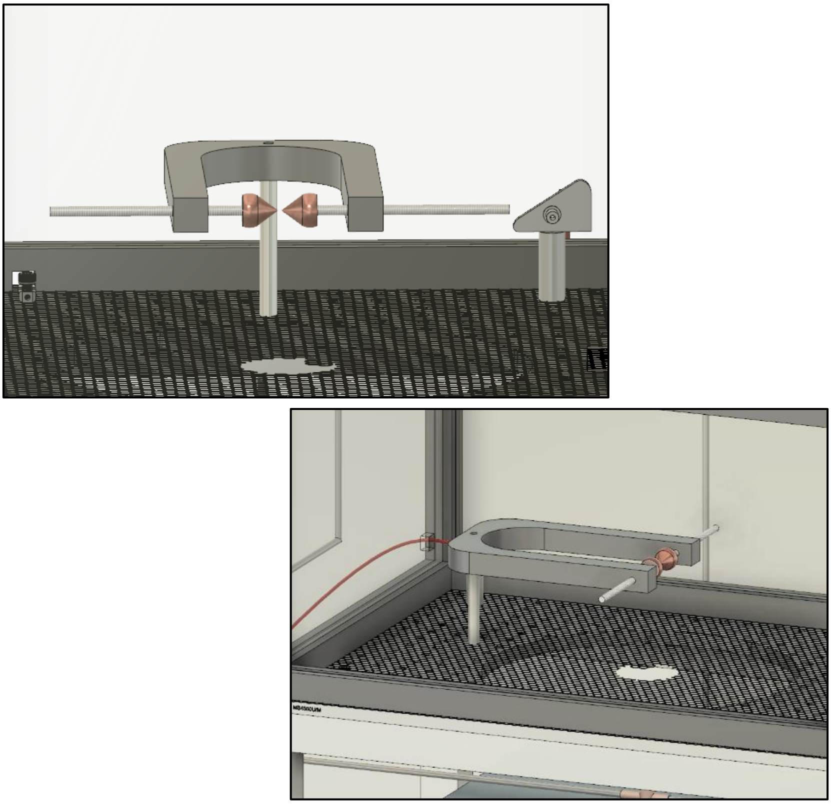

Figure 2.3: Front view (top image) and Side view (right image) of electrode setup in pre-study.

In order to make the experimental setup more dynamic and meet the needs of the experimental work planned out for the thesis research, this electrode setup had to be upgraded. Specific details and justification for altering the electrode setup will be described in Chapters 3 and 4.

2.3 Pre-study Results and Future Outlook

The pre-study experiment provided significant qualitative results regarding the trends of flame behavior as a result of the electrical discharge igniting the combustible battery vent gases. These trends were shown to be repeated in the experiment conducted in the scope of this work and will be explained in detail in Chapter 4.

The recommended future works, however, almost directly reflect the work done for this thesis research. Coming directly from [4] the ‘Future works’ section mentions the following four suggestions:

Predict flame behaviors employing chemical kinetics modeling

Investigate the impacts of the gas medium on creating/forming the discharge

Investigate the ignition phenomena by high-speed imaging (sampling rate >> 10kHz)

Investigate the effects of discharge on various vent gas mixtures employing laser-based diagnostics

As it will be seen in the following two chapters, these four suggestions from Subash are a mirror image of the motivation and research objectives of the two different experiments. The experiment detailed in Chapter 3 investigates the second suggestion, investigating the impact of the gas medium on the formation of electrical discharge. Through careful design and test case selection for the experiment detailed in Chapter 4, the other three suggestions were able to be met with one experimental setup.

3. Electrical Discharge in Different Gas Media

This section will provide a detailed explanation of the first of two experiments. First, the background knowledge necessary to obtain a general understanding of the theory behind the development and application of this experiment will be provided. Next, a literature review will provide insight into the current work being done by other researchers in this field. Third, the motivation and goals for this experiment will be described. Next, the experimental setup will be described, followed by the experiment's results. Finally, a discussion of the results can be found.

Note: This experiment, including its objectives, setup and results, were obtained in collaboration with Julia Lövgren.

3.1 Background Knowledge

This section will present the reader with the background knowledge necessary to have a basic understanding of the experimental motivation and results. As the experiments described in this chapter and in Chapter 4 have some overlapping topics, they will not be repeated in both chapters. Instead, all relevant background knowledge for the 'electric discharge in different gas media' experiment will be included here, and any information not mentioned that is specific to Chapter 4 will be mentioned there.

Batteries

All batteries store chemical energy and convert it into electrical energy through a series of chemical reactions. A battery consists of an anode, a cathode, an electrolyte solution and a separator. A basic schematic of a battery, also called an electrochemical cell, can be seen below.

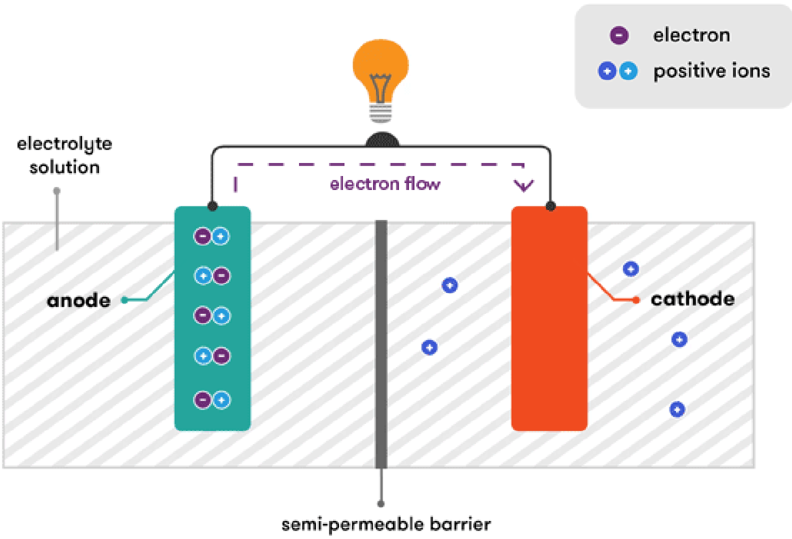

Figure 3.1: Basic schematic of a battery and main components [6]

Chemical reactions occur at the anode as it interacts with the electrolyte solution, creating electrons. At the same time, the cathode is interacting with the electrolyte, providing the cathode with the ability to accept electrons. The electrons then flow through a conductive wire, producing a current. As these chemical reactions are taking place and producing ions, a separator, seen in Figure 3.1 as the 'semi-permeable barrier,' prevents them from traveling freely between the anode and cathode. If this were allowed to happen, an electrical short circuit would occur [6].

Lithium-ion Batteries

Lithium-ion batteries (LIB) are dominating the battery industry due to their high energy density, quick charging capabilities and their longevity [2]. They are used in a majority of electronic gadgets, as well as the electric vehicle industry. LIBs utilize lithium atoms in the anode where they are ionized during a discharge cycle.

The properties and performance of any battery is highly dependent on the materials selected for each component. A common material for the negative electrode, or anode, is graphite or a compound known as Lithium Titanite, $Li_4Ti_5O_{12}$. A typical material used for the positive electrode, or cathode, is a transition metal oxide such as $Li(Ni_xCO_yMn_z)O_2$ or $Li(Ni_xCO_yAl_z)O_2$. These materials have been selected after years of research and performance analysis to optimize energy and power density, cycle performance and thermal stability [2].

The selection of the electrolyte is centered around ensuring smooth and rapid lithium ion transmission, and providing the proper chemical reactions when interacting with the anode and cathode. Typical electrolyte solutions used in the industry are comprised of organic solvents and salts dissolved within these solvents. Traditional commercial electrolytes comprised of organic carbonate solvent and $LiPF_6$ have been found to offer the best balance of electrochemical performance, costs and toxicity, as it is stated in [2]. These solutions, however, have caused some concern in terms of safety due to the flammability of the organic solvents.

Thermal Events/Thermal Runaway

The failure rate of LIBs under safe and proper operation conditions is extremely low, estimated to be 1 in 40 million [2]. However, batteries can often be overcharged, experience external heating or receive mechanical abuse. These events can cause a battery to experience thermal runaway.

Thermal runaway is an uncontrolled and self-propagating exothermic reaction within the battery that leads to rapid increase in temperature, venting of combustible gases and potential thermal events [7]. Thermal runaway is generally caused by internal short circuits, manufacturing defects, mechanical abuse, or exposure to high temperatures. The figure below provides a schematic depicting the stages and approximate temperatures associated with thermal runaway in a lithium-ion battery.

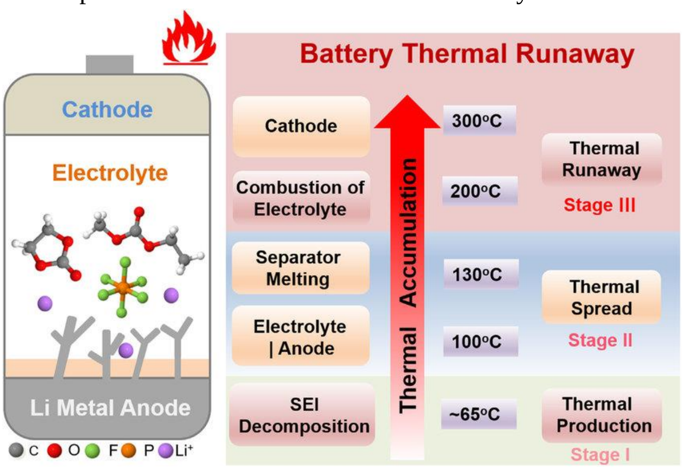

Figure 3.2: Schematic of thermal runaway in Li-ion batteries [8]

As external abuse happens to the battery, an internal short circuit can occur. This can be due to the separator being compromised, allowing direct contact between the anode and the cathode. As a result, the internal temperature of the battery rises quickly as the exothermic reactions between the electrolyte and electrodes occur, further deteriorating the battery. As the temperature increases, the intensity and rate of reactions increase, further amplifying the thermal runaway process. Flammable gases are released, posing a risk of fire or explosion.

Battery Vent Gases

The composition of the gases vented from a Li-ion battery in thermal runaway will vary depending on the state of charge, age, electrolyte composition and other properties of the battery. As the battery undergoes rapid temperature rise and exothermic reactions occur, the decomposing electrolyte generates various gases that are expelled through the battery's vents or ruptures in the battery casing.

The most common gases observed during thermal runaway of a LIB include carbon dioxide (CO_2), carbon monoxide (CO), methane (CH_4), hydrogen (H_2), and ethane (C_2H_6) [3]. The composition at which these gases are present in a gas mixture expelled from a battery is extremely significant in understanding the level of risk of ignition. Gas analysis techniques including gas chromatography and mass spectrometry can be used to identify the composition of these gases, providing researchers with the ability to assess the severity of thermal runaway effects and design their products accordingly [7].

Electrical Discharge

Electrical discharge refers to the phenomenon of electricity passing through a medium, typically a gas or vacuum, causing ionization of the medium and the emission of light or heat. It is the flow of electric current through a conducting medium, driven by the potential difference between two conductive surfaces. The behavior of an electrical discharge is influenced by many factors, some of which include voltage, gas medium, pressure, electric field intensity and electrode material [9].

Classifications of Electrical Discharge

There are many types of electrical discharges, classified by their behavior. A few of the most relevant classifications are listed are described below.

Electrical Arc

An electrical arc is a sustained discharge between two conductive electrodes, typically in the form of a plasma column. An electrical arc is caused by a high potential difference across a small gap and have high temperatures and luminosity. As the electrical arc occurs across this gap, the gas medium is ionized, creating a channel for the electrons to travel. The high temperatures of this arc create a localized heat source, providing more than enough heat for potential ignition of flammable gases [10].

Spark Discharge

Spark discharges are classified as a quick, non-self-sustaining discharge that provides a sudden release of electrical energy. Spark discharge occurs when the potential difference between two electrodes exceeds a critical value, and the surround gas medium is ionized, creating a visible discharge [9]. Compared to arcs, spark discharges typically have a lower energy and are commonly found in spark plugs, electrical switches and other applications in which a low amount of nearly instantaneous energy is required [11].

Corona Discharge

Corona discharges are moderately low-power electric discharges that occur near atmospheric pressure. They are characterized by their low-intensity, non-luminous discharge that occurs when the electric field strength exceeds a critical value. This type of discharge is common in high-voltage power transmission lines and transformers [12]. Visually, a corona discharge appears as a faint glow or a halo-like structure surrounding a conductor.

Gliding Arc

Gliding arc discharges are high-velocity plasma discharges that propagate along a diverging or converging electrode configuration. They are classified as non-thermal, meaning the gas medium is only partially ionized. This results in an overall lower temperature than the previous classifications of discharge. Gliding arcs show a gliding motion along the surface of the electrode, hence the name. This gliding motion generates reactive species and various plasma chemistry effects, making it useful in fields such as plasma-assisted combustion and material processing [13]. Gliding arcs are seen to occur near or at atmospheric pressure.

Breakdown

Electrical breakdown, or dielectric breakdown, is the sudden intense increase in electrical conductivity in a gas medium. This is due to exposure to a sufficiently high electric field. Electrical breakdown can lead to the aforementioned electric discharge, such as a spark or electrical arc [14]. Quantifying and predicting electrical breakdown in specific gases is a complex field of study. The following topics present a few theories related to doing so.

Townsend Model and Coefficients

The Townsend Model is a theoretical model that describes the electrical breakdown in gases based on ionization. Under an applied electric field, the model explains how the ionization of gas atoms occurs [15]. The Townsend coefficient, or the ionization coefficient, denoted α, describes the rate of ionization per unit distance traveled by an electron in a gas under the influence of an electric field. The higher the value of α, the higher the probability of gas ionization occurring.

Paschen Curve

A Paschen curve, seen in Figure 3.3 plots the minimum breakdown voltage as a function of the product of pressure and distance between electrodes. This curve is applicable to gases in low pressure, in the range of approximately 10 to 1000 Torr [15]. As it can be seen, when the product pressure and distance is extremely small, the minimum breakdown voltage is quite high. As stated in [15], this is attributed to the fact that under a critical value of the p*d product, the discharge will occur between the longer of two paths. However, above this critical value, the breakdown voltage gradually increases as the product increases.

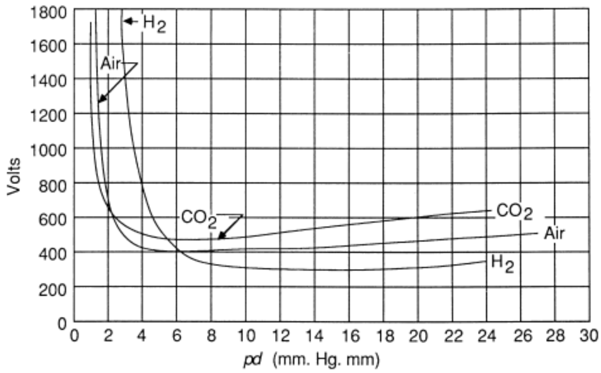

Figure 3.3: Paschen curve [15]

3.2 Literature Review

This section will provide a brief summary of a few literary sources related to the topic of this experiment.

Experimental investigation of breakdown voltage of CO_2, N_2 and SF_6 gases, and CO_2-SF_6 and N_2–SF_6 mixtures under different voltage waveforms [16]**:** This scientific paper presents a comparative study of the breakdown voltage of different gases under different voltage sources. It notes that SF_6 is a very effective insulator but has some detrimental greenhouse effects. Using a sphere-to-sphere electrode arrangement, three different voltage sources were used to test the breakdown voltage. The results showed that SF_6 had the highest breakdown voltage, and combining SF_6 with other gases like CO_2 and N_2 increased the breakdown voltage. It also notes that gases have different values for minimum breakdown voltage for AC and DC voltage.

Synergistic Effect of SF_6 and N_2 Gas Mixtures on the Dynamics of Electrical Breakdown [17] **:** The research presented in this scientific paper investigated the combined impact of SF_6 and N_2 gas mixtures on the behavior of breakdown voltage. The objective was based on understanding the synergistic effects that occur when these gases are combined. The dynamics of electrical breakdown were examined experimentally, providing valuable insights for various applications that require electrical insulation. The results conclude that the synergistic effects are almost completely lost when the 'rate of rise' is high. It states the synergistic effects are most prevalent at certain compositions of the mixture and is greater at higher pressures.

3.3 Motivation and Methodology

The information in this section provides a more applied and practical explanation for the motivation behind this experiment. This section combines the theory obtained through extensive literature research with the practical desired outcomes that can be considered useful information for both industry and academic use. The justification of experimental design is explained in this section, while the physical experimental design used to accommodate the specific needs in the laboratory are explained in the following section, Section 3.4.

Experiment Motivation

As it was outlined in Section 1.1, any high voltage system is susceptible to electrical discharge depending on a number of different factors. Understanding the different factors that contribute to the frequency and 'strength' of electrical discharge can be critical in minimizing the risk associated with this phenomenon. In electrical vehicle batteries, certain gases can collect in the venting areas near the battery systems, especially in the case of a thermal event. This presents a significant number of unknowns:

> Will this lead to arcing more frequently than when the venting path is only filled with atmospheric air?
>
> Will these gases always ignite in the event of electrical discharge?
>
> Where will the electrical discharge occur?

All of these questions present a different parameter within the system that can influence the impact an electrical discharge may have in any given scenario. In order to develop a baseline for understanding these questions, this experiment was designed to test the impact a number of parameters had on the breakdown voltage.

Experiment Goals

Based on the information presented in the previous section, a number of goals were decided upon for this experiment. First, it was important to identify which parameters were able to be controlled and changed, while recording meaningful information to identify a corresponding trend. As it was mentioned in Section 3.1, breakdown voltage is the minimum voltage value at which electrical discharge will occur. Therefore, the ability to accurately record voltage and current coming from a power supply at the moment of electrical discharge provides the opportunity of varying other parameters to represent possible scenarios in the event of a discharge. As it is detailed in the Appendix , a voltage and current probe made it possible to do this.

In the case of battery venting, the area in between the conductive surfaces with high potential difference changes tremendously. To understand how this will impact the electrical discharge, different gases can be flown in between electrodes. As the gas between the electrodes changes, the breakdown voltage is expected to change. The objective of this experiment is not necessarily to identify a specific value for the breakdown voltage of a specific gas under different circumstances. The objective, rather, is to gather data and identify trends that can provide an understanding of how the minimum breakdown voltage may increase or decrease based on a number of varying parameters. With this information, future works may build on the identified trends and improve the understanding of electrical discharge across different gas media.

Experiment Methodology

As it was mentioned in the Experiment Motivation, the research questions present a number of different parameters that will alter the behavior of electrical discharge. The next step in designing this experiment was to select the parameters that could be changed with precision and have a direct impact on the minimum breakdown voltage.

Referring back to the Paschen curve (Townsend Model), the product of pressure and distance play a vital role in determining the value of minimum breakdown voltage of a gas at low pressures. Because the gases in the case of this experiment are flowing out of a quartz mixing tube before being exposed to the electrical discharge, it can be assumed that these gases will be near atmospheric pressure in all cases. So, considering a constant pressure across all cases, varying the **distance** between electrodes provides an opportunity to recreate the Paschen curves for the different gas media in this experiment.

It is a well-established fact that a number of gas properties are heavily dependent on temperature. Additionally, it was mentioned in Section 2.1 that there is a possibility of two main expulsions of vent gases in a Li-ion battery undergoing a thermal event. This means that at any given time in a thermal event, a battery vent system within an electrical vehicle can be filled with gases of varying temperatures. Considering all this, it is extremely important to be able to determine the dependence of the minimum breakdown voltage on the **temperature.**

The two gases mentioned throughout this research paper, LFP and NCA, are only two cases in a multitude of possible battery vent gas compositions. Because the gas compositions can vary drastically between different battery chemistries, identifying a trend of the minimum breakdown voltage with respect to gas composition can provide a significant starting point for further research in this area. However, due to the incredibly high number of chemical reactions between elements within these gas mixtures occurring within during the electrical discharge/vent gas interaction, it is necessary to understand the possibility that the breakdown voltage can vary greatly between gas mixtures. For this reason, it was decided that in order to investigate this interaction at as fundamental of a level as possible, elemental gases should be analyzed also. Varying the **gas composition**, like varying the equivalence ratio, should provide valuable insight into the chemical properties impacting the minimum breakdown voltage.

Finally, the **flow rate** was varied to analyze the impact this would have on the breakdown voltage of a flowing gas. In the event that gases are expelled from a battery vent or rupture, the rate at which these gases event can vary. This is largely dependent on the pressure (and consequently, the temperature) within the battery. Both of these variables can result in a wide range of gas flow rates. For this reason, these measurements can provide valuable insight into determining the likelihood of an electrical discharge occurring in certain venting situations.

Experimental Terminology

This brief section will explain terms used in the remainder of this chapter.

Trigger event: When obtaining measurements for this experiment using the oscilloscope and probes, a trigger value must be set. In this case, the trigger value was set at a low current, around 0.5A. As electrical discharge occurs, the current spikes, the setpoint of the current is reached, and the oscilloscope begins gathering data. The beginning point of data collection is known as a trigger event. In this experiment, the oscilloscope was programmed to capture between 50-100 trigger events, with 500,000 data points for each trigger. There was a time span of 40 nanoseconds in between each data point.

Understanding the Measurements

This section will provide the reader with a general understanding of the accumulation of data in order to clarify the data analysis process. Across all measurements, a few similar occurrences can be observed. In Figure 3.4, the measurements taken from the oscilloscope for voltage values can be seen. Voltage, shown in the yellow line, builds up in the capacitor bank. Once it reaches a minimum value, established herein as the minimum breakdown voltage, electrical discharge occurs (seen as ‘breakdown event 1’). This discharge creates an ionized channel for current to travel. The voltage then dissipates and begins to recharge in the capacitor bank. This can be seen in the figure below as well.

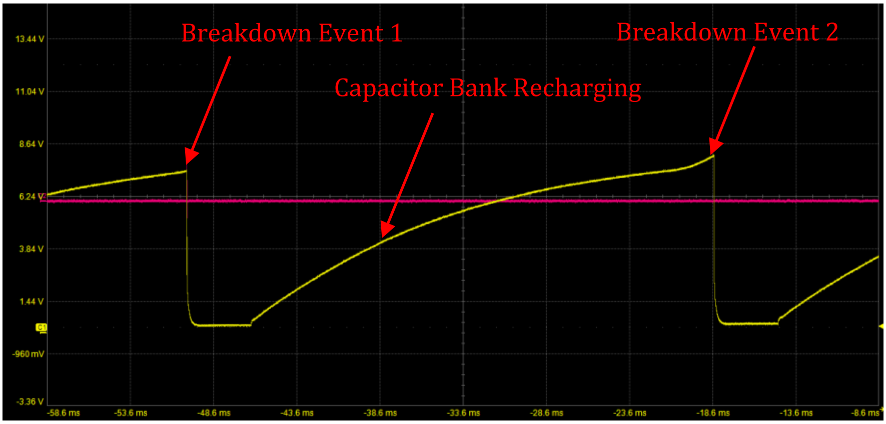

Figure 3.4: Oscilloscope measurement showing voltage during breakdown

Another common phenomenon that was observed involved the oscillation in the measurements gathered for both the current and voltage. As it can be seen in the post-processed, enlarged sample of current data collected in Figure 3.5, oscillation was found in all measurements.

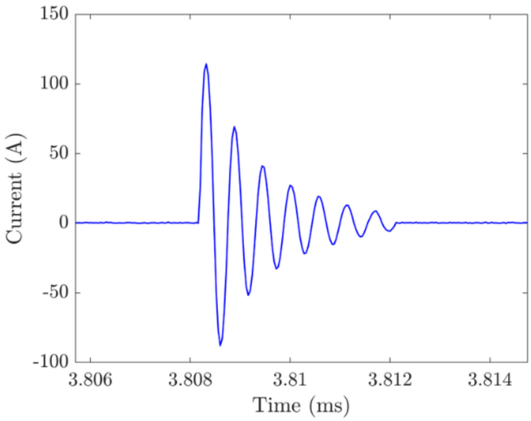

Figure 3.5: Observed oscilloscope oscillation

Although this oscillation can only be seen at a high zoom-scale, it is worth mentioning as it can be caused by a number of factors including bandwidth, resolution, input impedance, or signal conversion [18]. The exploration of this phenomenon was not explored further within the scope of this report, but it was also noticed that as the parameters of the flowing fluid were changed, the magnitude and frequency of the oscillation also changed. As this can provide further insight into the interaction of the electrical discharge, this information will be recommended as a future study in the Future Outlook section.

As it was discussed in Section 3.1, the Paschen curve implies a direct correlation between the distance of the electrode gap and the minimum breakdown voltage. The following Figure 3.6, one of many comparison cases created, is used to demonstrate this overall trend. Although this figure does display important information and will be shown again later in the chapter, it is placed here to provide the reader with an explanation of how to interpret the figures that will be presented in the remainder of this Chapter.

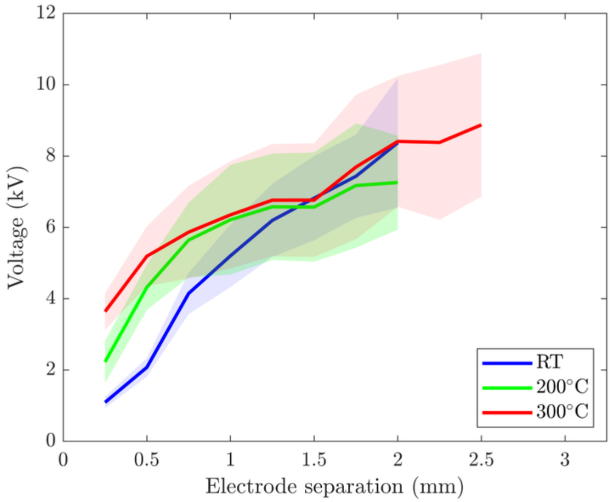

Figure 3.6: LFP gases with 80% N_2, flow velocity of 5 m/s

The legend provided displays the corresponding temperature of the gas mixture. The shaded regions correspond to the standard deviation of the respective data line. In all figures throughout this chapter, the standard deviation displays indicates +/- one standard deviation.

Case Selection

With the obvious dependence the minimum breakdown voltage has on the separation distance between the electrodes, it was decided that the voltage should be measured at increments of 0.25mm-3mm, while varying different parameters. By doing this, it is possible to identify the impact of these different parameters on the breakdown voltage and determine the magnitude of this impact as the breakdown voltage increases.

The parameters chosen to vary were temperature, gas flow velocity and gas composition as mentioned in Section 3.3. Table 3.1 shows the complete table of different gases and the conditions at which they were tested in this experiment.

Gas Composition

There are various literature sources describing the ionization coefficient, α, of certain elemental gases and their tendency to breakdown. However, there is no agreed-upon method of calculating α for gas mixtures, making it difficult to predict breakdown voltages of gases with different compositions. As it was described in Section 3.2, experiments have been performed to analyze and predict the breakdown voltage in gas mixtures and have been presented, but not necessarily accepted in academia or industry. For this reason, it was decided it would be beneficial to begin by measuring the minimum breakdown voltage of elemental gases O_2 and N_2. Next, in order to provide an opportunity for future researchers to test out the plausibility of these mixture rules, a gas mixture of both N2 and O2 were tested, replicating air. Of course, air contains other elements in lower concentrations, but for the sake of this experiment, only these two elements were included.

In order to provide valuable information in regard to battery vent gases, it was also necessary to include the NCA and LFP vent gases. However, as these gases are flammable and the heat would likely damage the probes or interfere with measurements, they needed to be mixed with an inert gas to prevent ignition. As seen in Table 3.1, the gas mixtures to represent the battery vent gases consisted of 20% NCA or LFP gas, and 80% N_2.

Still-standing air was also measured to represent the breakdown voltage of a system that does not have battery gases being vented into it. This was used a baseline and provides some useful information, but due to the inability to have the other gases in a still-standing environment, it is difficult to make comparisons as the effect of flow velocity changes the measured breakdown voltage.

Temperature

The breakdown voltage was recorded at room temperature (denoted RT in Table 3.1), 200 °C and 300°C. Room temperature in the lab was measured to be 19 °C. Room temperature and 300 °C were selected to represent two extremes, providing the most apparent changes in breakdown voltage as a result of temperature. 200 °C was selected as an intermediate value.

Measured Parameters			
Gas	Temperature (°C)	Flow Rate (m/s)	Distance (mm)
Still standing Air	RT	5	0.25 - 3
O2	RT, 200, 300	5	0.25 - 3
N2	RT, 200, 300	2.5 (RT only), 5	0.25 - 3
21% O2 & 79% N2	RT, 200, 300	5	0.25 - 3
NCA & 80% N2	RT, 200, 300	5	0.25 - 3
LFP & 80% N2	RT, 200, 300	5	0.25 - 3

Table 3.1: Case selection for Discharge Experiment

3.4 Experimental Setup

The addendum found in Appendix A, "Experimental Setup," provides an overview of the entire setup. This addendum was created in collaboration with Julia Lövgren as a shared document, and for this reason is found in the Appendix rather than in the main body of this report. It is suggested that the reader views the addendum first to gain an overall understanding of the experimental setup. This section will provide details pertaining to certain design choices not mentioned in the addendum.

Improvements From Pre-Study

This section discusses changes made to the experimental setup from the pre-study setup created by Arman Subash, detailed in Section 2.2.

Electrode Setup

Considering the need of this experiment to precisely alter the distance between electrodes, some improvements had to be made to the electrode setup from the pre-study. First and foremost, the "U" shape Teflon block used to mount the electrodes had to be split into two separate mounts, with one placed on a translational stage. A description of this solution can be found in Appendix A.

A side view of the new electrode orientation and motor mount can be seen below. It can be seen that the orientation of the electrodes also changed. While in the pre-study, the orientation was perfectly horizontal as shown in Figure 2.3, they needed to be reoriented to accommodate the path of the laser sheet used for Julia Lövgren's OH-PLIF measurements for the experiment in Chapter 4. An explanation of the necessity of minimizing electrode interference in the path of the laser sheet can be found in [5].

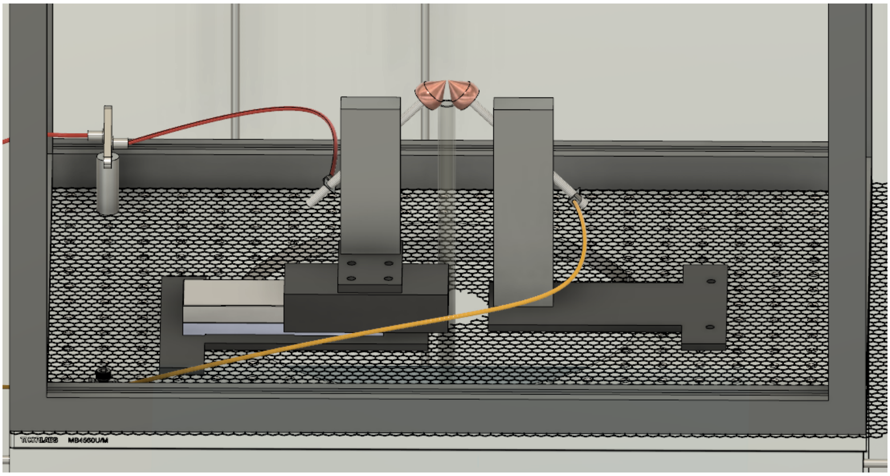

Figure 3.7: Side view of update electrode setup

Measuring Current and Voltage

While this is not necessarily an improvement made on the experimental setup from the pre-study, it is an important change made. As it has been mentioned, the main goal of this experiment is to record the current and voltage of the system at the moment electrical discharge occurs. Details regarding the equipment used to do this can be found in Appendix A.

Software

A multitude of programs were used to control different pieces of equipment used to perform this experiment. This section will provide a brief description of each software used.

APT User

The Thorlabs motor was controlled remotely using software provided by APT. Two separate programs were used, one to establish a connection signal between the computer and the motor, and one to send commands to control the motor. A screenshot of the latter, APT User, can be seen in the following figure.

Figure 3.8: APT User Software used to control translational stage

In controlling this motor, the distance between the electrodes was able to be varied at extremely small and precise measurements. The software, in combination with the Thorlabs motor, has the ability to move in increments as small as 0.05 microns with great precision. It can be seen in the Case Selection subsection, however, that intervals of 0.25 mm were used.

WaveStudio

The Teledyne Lecroy oscilloscope used to collect signals from the voltage and current probes implemented WaveStudio software. This software provided the display and control of the measurements being taken. Using this software, it was possible to set minimum trigger values for the voltage, telling the oscilloscope at what setpoint to start collecting data. A screenshot of this software can be seen in the following figure. This is an example reading of two electrical discharge events, showing voltage and current. The data shown below represents an accumulation of 100 trigger events.

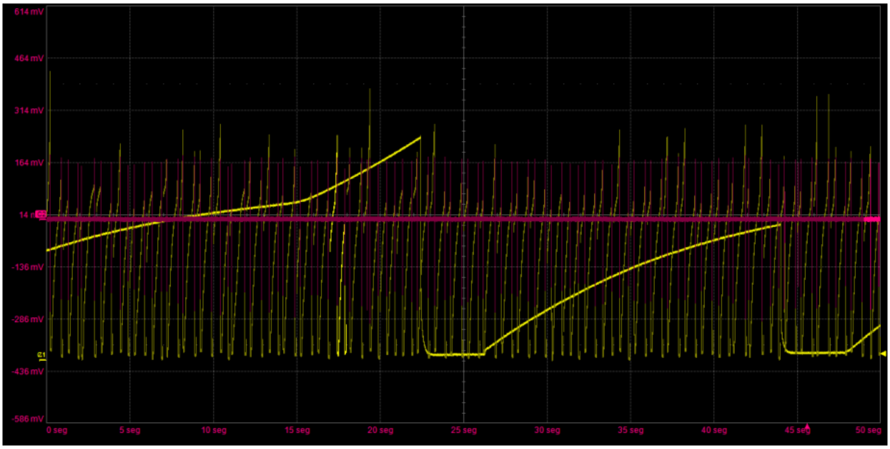

Figure 3.9: WaveStudio software used to collect data from oscilloscope

FlowView

Mass flow controllers (MFCs) from Bronkhurst were used to control the flow of gases through the three-line configuration. A description of these MFCs can be found in the addendum. The software used to control the MFCs is called FlowView. FlowView enables the user to remotely operate the MFCs simultaneously with great precision and quick response time. This software is instrumental in both experiments performed as precise amounts of gas are needed to provide a specified equivalence ratio and flow rate. This software is the only one mentioned in this section that was used in both experiments.

Note: The electrode setup detailed in this section and in the Appendix was not changed between this experiment and the experiment laid out in Chapter 4. The current and voltage probes were removed, however.

3.5 Results and Discussion

Breakdown Voltage Trends

As it was mentioned in Section 3.1 explained by the Paschen Curve, and in Section 3.3 with the explanation of case selection, increasing the distance between the electrodes increases the minimum breakdown voltage. This can be expected, as the increased distance results in an increased volume of gas which must be ionized. This trend can be clearly seen in Figure 3.10. Regardless of the gas media, this increased volume represents an increased resistance. Therefore, it is reasonable to conclude that a higher voltage is required to produce a current between the electrodes. The rate at which these breakdown voltages increase varies as different parameters change, as it can be seen in Figure 3.10 across the three different temperatures. This effect, and the effect of varying the other aforementioned parameters, will be discussed in the following sections.

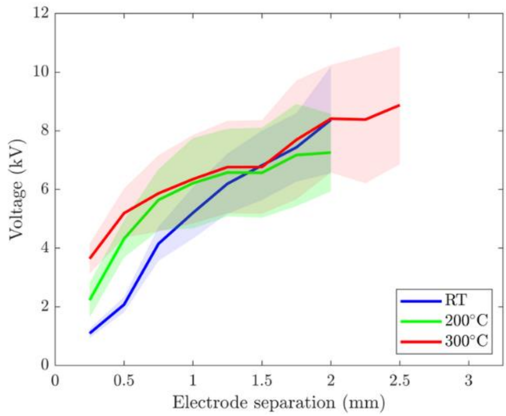

Figure 3.10: Breakdown voltage of LFP gas at varying temperatures

Effect of Temperature

Figure 3.11 displays the effect of varying temperature on the breakdown behavior of LFP and N_2 at a gas flow velocity of 5 m/s. For the LFP gas mixture, the breakdown voltage at room temperature (19 °C) is notably lower than it is at 200 and 300 °C until approximately 1.5mm separation distance. Around this point, the values converge and follow a similar trend. For pure N_2, the opposite appears to be true. The breakdown voltage is lower throughout all of the separation distances for 200 and 300 °C, with no obvious convergence with the room temperature values at any point.

The plot for N_2, seen on the right in Figure 3.11, includes two different data sets gathered for N_2 at room temperature. These parameters were simply recorded twice on different days in an effort to test the replicability of data being gathered. Interestingly, it can be seen that while the values do not show an exact match, the data collected follows the exact same trend. This can likely be attributed to the 'conditioning' of the experimental setup to be more prone to electrical discharge. In other words, as the tests were performed continuously throughout the day, the electrodes were continuously rising in temperature. Although this was gradual, the increase in temperature means there was not an exact match in the conditions of all components involved in the formation of discharge. Ultimately, the objective of this experiment was to understand the trend of the breakdown voltage as temperature was varied, which remained the same in both cases. Further exploration into the impact of continuous testing is necessary to verify any results in future experiments of a similar nature and determine the sensitivity of the system to gradual temperature change.

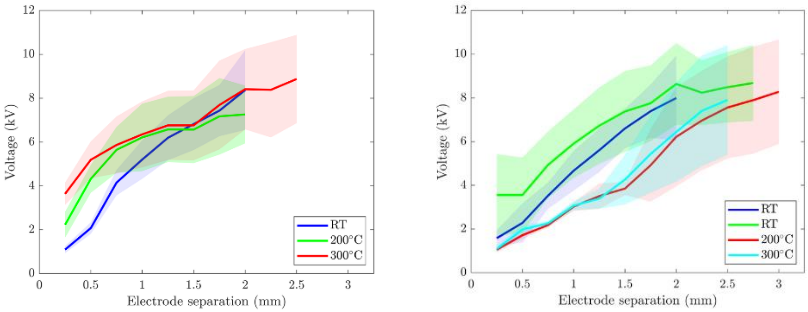

Figure 3.11: Breakdown voltage trend with varying temperatures of LFP gas (left) and N_2 (right)

Effect of Gas Mixture

The minimum breakdown voltage of different gases in room temperature conditions can be seen in Figure 3.12, while the images in Figure 3.13 show the breakdown voltages of the LFP and NCA gases at room temperature and 300 °C, respectively.

It should be noted that Figure 3.12 demonstrates a relatively high standard deviation for the values collected, and suggests further testing is needed to confirm the results. However, it can be seen from the general trend that the individual gases, N_2 and O_2 have a noticeably lower breakdown voltage value than that of the N_2 and O_2 mixture. One likely cause of this is the effect of gas mixture synergism. Synergism states that the breakdown strength of a mixture is either higher or lower than that of the constituent gases due to the interactions between molecules. Because this effect can either increase or decrease the breakdown value, further research must be done to draw concrete conclusions.

In Figure 3.13, it can be seen that the breakdown voltage of NCA is higher than that of LFP for the majority of the separation distances at room temperature. Interestingly, the opposite is true for the two gas mixtures at 300 °C. With further research into these gas mixtures dielectric properties, it may be possible to justify the similarities between these values.

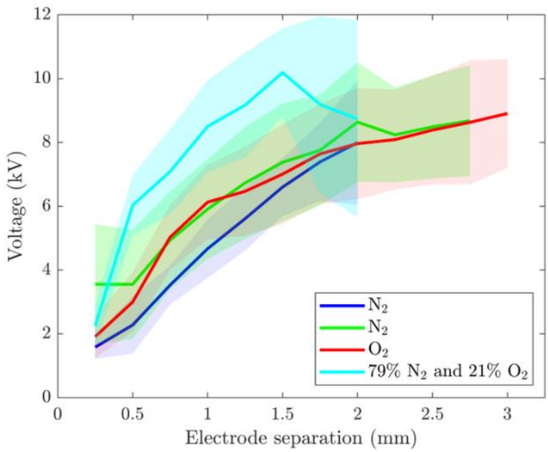

Figure 3.12: Breakdown voltage of different gases at room temperature with flow velocity of 5 m/s

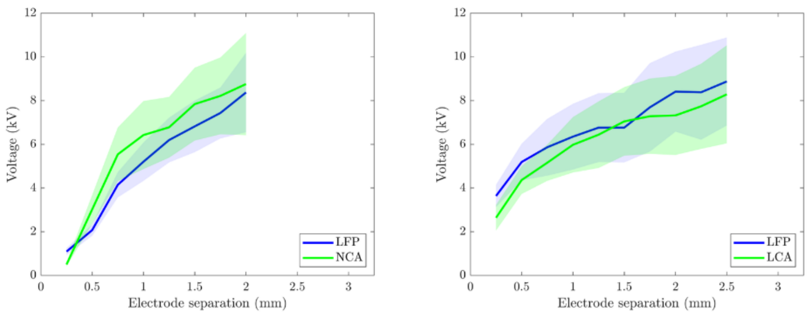

Figure 3.13: Breakdown voltage of LFP and NCA gases at room temperature (left) and 300 °C (right), flow velocity of 5 m/s

Effect of Gas Flow Velocity

Figure 3.14 displays the results of varying the gas flow velocity of pure N_2 at room temperature. Flow velocities of 2.5 and 5 m/s were analyzed, with no distinguishable differences between the two velocities. Increasing the flow velocity is expected to promote the movement of charged particles and enhance electron diffusion within the gas medium. For this reason, it is reasonable to expect higher voltage would be required to increase the concentration of electrons needed to produce an ionized channel. Additionally, higher flow velocities tend to decrease the mean free path of electrons, meaning a shorter average distance between collision events with gas molecules [9]. This will reduce the amount of energy they are able to gain, reducing the probability of ionization and the formation of an ionized channel. Further studies will be needed at higher flow velocities to confirm these theoretical relationships.

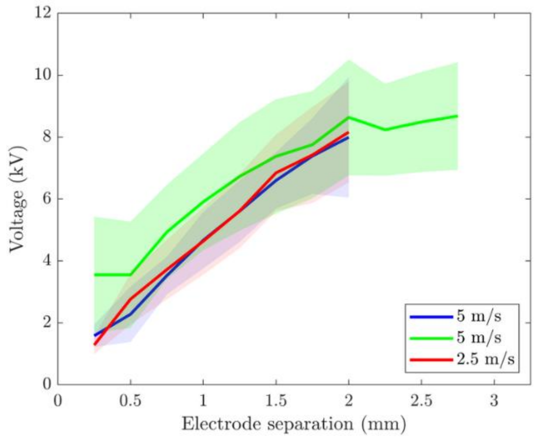

Figure 3.14: Breakdown voltage of N_2 gas at room temperature at flow rate of 5 m/s and 2.5 m/s

Figure 3.15 does in fact support this claim, however. This plot compares the breakdown values of still-standing air, and a gas mixture made to represent the primary constituents of air in the appropriate ratio (79% N_2 and 21% O_2) flowing at 5 m/s. The flowing gas mixture exhibits a higher breakdown voltage at all distances, likely due to the previously mentioned effects. It can also be seen that at around 1.5mm, the breakdown voltage begins to decrease. Further investigation may be able to indicate if this is a replicable trend, or if it is due to the aforementioned conditioning of the experimental setup.

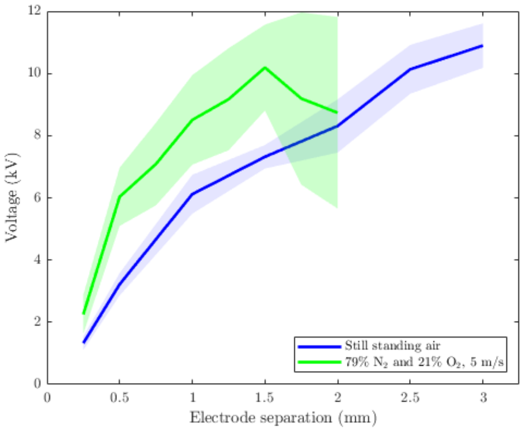

Figure 3.15: Breakdown voltage of still-standing air and gas mixture representative of air (79% N_2 and 21% O_2) flowing at 5 m/s

3.6 Conclusion and Future Outlook

This section will describe the possible areas of research that may increase understanding of the phenomena observed in this chapter.

Electrical Discharge Conditions

The results presented in this chapter indicate some general trends of breakdown voltage as various parameters are changed. In general, the observed trends followed expectations based on the applicable theories. However, it must also be noted that only two gases were tested. While these were selected to be representative of a highly reactive and less reactive gas mixture vented from a battery experiencing thermal runaway, there are obviously many more gas mixtures that can be studied.

As it was noted in the results of the gas mixture effect on the breakdown voltage, synergistic effects seem to play a vital role in the breakdown voltage value. For this reason, it is suggested that experiments and literature be explored to increase understanding of the synergistic effects taking place within a variety of battery vent gases.

Industry Outlook

Considering the importance of locating areas within a battery system that are prone to experience electrical discharge, steps should be taken to increase understanding of this phenomenon. One limitation of this experimental setup is the constraint of the electrodes. Of course, these were very useful in the scope of the experimental objective laid forth, but in order to gain a better understanding of possible locations, the experimental setup must be adjusted.

Simulations and software that can calculate the likelihood of a discharge forming in certain conditions can be utilized to improve knowledge in this area as well. COMSOL Multiphysics plasma module provides the capability of importing certain geometries and materials and defining a gas medium to analyze electric field parameters.

Experimental Limitations

As in any experiment, understanding the replicability of an experiment's results is vital in confirming test accuracy. Changing a number of different parameters to perform tests increases the dependence on system consistency. In other words, the more the gas flow is being altered and changed, the more important it is to have robust and precise equipment within the system. Upon review of this experiment, a few possible sources of error can be considered.

As it can be seen in Figure 3.12, tests for N_2 were run twice. This was done with the intention of analyzing the replicability of the tests. One test was completed in the morning, before any other experiments were performed using this setup. The second test was completed at the end of the day, after consecutive hours of testing. It can be seen that the breakdown voltage between the two are different, indicating inconsistent results. It is important to note that the trend remains the same, so the results are not rendered insignificant. However, due to the difficulty replicating results, it should be considered in future endeavors that the robustness of the system needs to be improved.

The most likely and most significant cause of this inconsistency is expected to be electrode conditioning. As the system is running and high levels of current pass through the electrodes, they begin to warm up. As the temperature of the conductive material increases, the required voltage to produce electrical breakdown decreases. The difficulty in limiting this effect is that the extreme temperature of the electrical discharge increases the surface temperature of the electrodes so drastically that it would take hours for the surface to return to its initial temperature. Therefore, it was decided to continue with the experiments and keep note of the conditioning effects.

4. Identifying Combustion Trends Across a Range of Flow Parameters Using High Speed Imaging

The term 'combustion trends' as it is found in the title of this chapter, and as is explored in this experiment, refers mainly to two specific phenomena: The ignition event and the flame behavior of a gas. This section will provide an in-depth description of the second of the two experiments performed. It will follow the format of Chapter 2, including the experiment's motivation, relevant background knowledge, literature review, experimental setup, results and discussion.

Note: This experiment, including its objectives, setup and results, were obtained in collaboration with Julia Lövgren. Lövgren's report, however, utilized laser diagnostics to obtain OH-PLIF images of the same test cases, rather than high-speed imaging. A brief explanation of the laser diagnostics goals and setup can be found in this section, but for a more in-depth description, please reference Lövgren's thesis paper, "Discharge and Flame Chemistry in Lithium-Ion Battery Vent Gases - Investigations using Breakdown Experiments with Laser-Based Diagnostics."

4.1 Background Knowledge

This section will present the reader with the background knowledge necessary to have a basic understanding of the experimental motivation and results. Some of the information in Section 3.1 is applicable to this chapter as well. This experiment utilizes some results from [5]. Please reference this document to obtain background information regarding the OH-PLIF laser diagnostics.

Combustion

Combustion is a chemical reaction that occurs between a fuel and an oxidant, typically oxygen, resulting in the release of heat and the production of products such as water, carbon dioxide, and other gases. There are two primary modes of ignition in combustion: self-ignition and spark ignition. Self-ignition occurs when a fuel spontaneously ignites due to high temperature, pressure, or chemical reaction. This can occur in engines, where the compression of a fuel-air mixture can cause it to self-ignite. Spark ignition, on the other hand, involves the use of a spark to ignite a fuel-air mixture [1].

Equivalence Ratio

The equivalence ratio, denoted Φ, is a critical factor in combustion, as it determines the amount of oxygen available for the reaction. The stoichiometric equivalence ratio is the ratio of air to fuel at which there is exactly enough oxygen to completely burn the fuel. If there is too little oxygen, the fuel will not completely burn, resulting in the production of pollutants such as carbon monoxide and unburned hydrocarbons. If there is too much oxygen, the excess oxygen will not participate in the reaction, reducing efficiency and increasing emissions of nitrogen oxides. As stated in [19], the equivalence ratio can be determined by the following equation:

$$\Phi = \frac{(A/F)_{stoic}}{(A/F)} = \frac{(F/A)}{(F/A)_{stoic}}$$

Pre-mixed Flames

Pre-mixing is a technique used to ensure that the fuel and oxidant are thoroughly mixed before combustion. This can improve the efficiency and performance of combustion processes, as well as reduce emissions of pollutants. In internal combustion engines, pre-mixing is achieved by mixing fuel with air before it enters the combustion chamber. Pre-mixed flames can be characterized by several parameters, including laminar flame speed, flame stability, and flame structure [1].

Diffusion Flames

Diffusion flames are a phenomenon in which fuel and oxidizer come together in a reaction zone through turbulent and molecular diffusion [20]. In contrast to a pre-mixed flame, the fuel and the oxidizer interact at the flame front, resulting in a uniquely identifiable flame structure. A key method in identifying diffusion flames is identifying the species concentration (i.e., using OH-PLIF).

Flammability Limit

The flammability limit of a fuel defines the range of equivalence ratios at which the fuel and oxidizer mixture will undergo combustion. The lower flammability limit is the minimum equivalence ratio at which combustion will occur, and the upper flammability limit describes the maximum. The flammability limit of a fuel depends heavily on the chemical composition of the fuel. Fuels with higher energy content and lower ignition temperatures generally have wide flammable ranges [1].

4.2 Motivation and Methodology

The two gases selected to be representative of the higher and lower explosive gases, NCA and LFP, were mentioned to have come from research conducted by Elna Nilsson due to their prevalence in Li-ion batteries usage. As it is mentioned in Section 3.1, the first expulsion of vent gases in a Li-ion battery undergoing a thermal event usually occurs around 150 °C. A second expulsion of vent gases is common, usually occurring around 300 °C. For this reason, as it can be seen in Figures 4.1 and 4.2, these tests were executed with gas temperatures of 150 and 300 °C.

One of the main areas of focus in combustion behavior is the equivalence ratio. Changing the amount of fuel or air in a mixture can drastically impact combustion rates, flame temperatures and flame behaviors, among several other things. While it is difficult to pinpoint the equivalence ratio of the battery vent gases within the venting system at the point of ignition, it is important to determine any type of trend in the ignition event and flame behavior with varying equivalence ratios. This can provide a good foundation for understanding chemical reactions when an electrical discharge interacts with a combustible gas, and in combination with chemical kinetics modelling, can provide useful information to be able to predict certain behaviors.

Similar to the experiment in Chapter 3, temperature and gas composition effects are also extremely important to analyze in order to understand these phenomena as they relate to battery safety. For this reason, this experiment will investigate trends of combustion and ignition as equivalence ratios, temperature and gas composition vary.

Case Selection

As in the experiment detailed in Chapter 3, selecting specific cases to provide meaningful comparisons were paramount. As it was previously mentioned, the parameters being varied included the gas temperature (150 °C and 300 °C), gas flow velocity (5, 10 and 15 m/s), equivalence ratio (0.8-4) and the gas composition (NCA and LFP). Recording and saving the data required for the high-speed images at two different frame rates across a high number of test cases could be very time consuming. To streamline this, a 'working scan' was performed to gain a basic understanding of the flame behavior.

To complete this scan, no recordings were being conducted. Rather, the flame behavior was noted for each gas, at each flow rate, at each temperature while varying the value of the equivalence ratio progressively from 0.8 to 4. In doing so, it was possible to gain an understanding of the expected flame behavior, making it possible to better determine which cases should be further investigated. These cases were then analyzed with high-speed imaging and OH-PLIF laser diagnostics. Figures 4.1 and 4.2 show the flame behavior of the LFP and NCA gas mixtures for the different cases over a range of equivalence ratios.

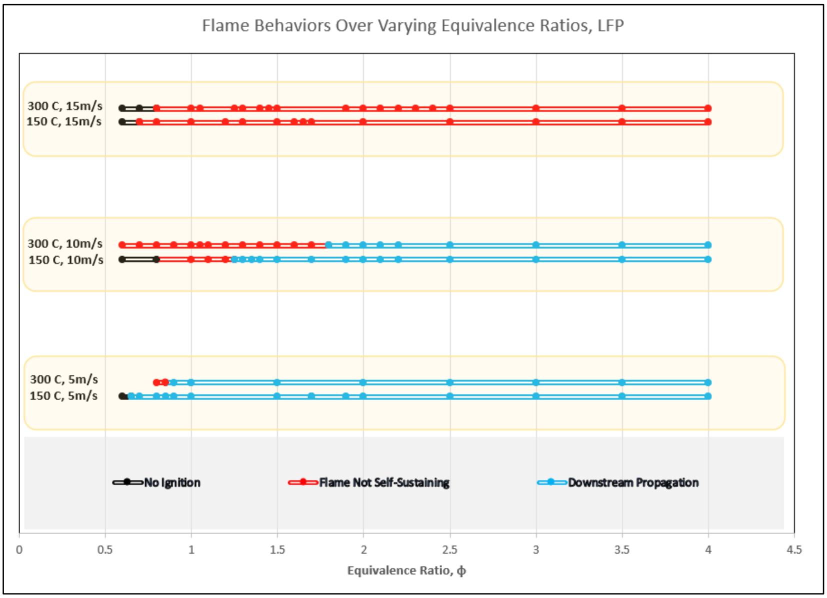

Figure 4.1: Flame behaviors for LFP gas mixture

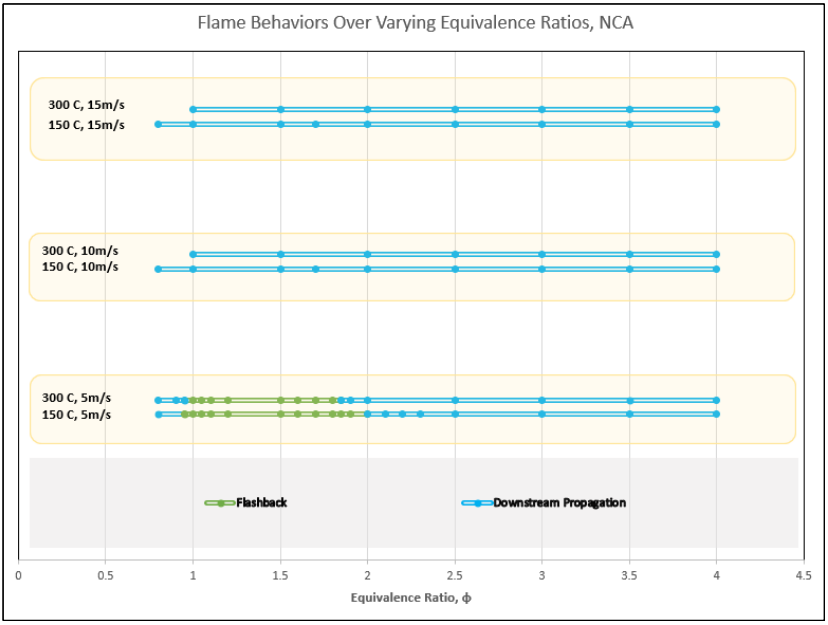

Figure 4.2: Flame behaviors for NCA gas mixture

Using the above figures, it is possible to determine any transition points where the flame switched from one behavior to another. These cases, along with a few intermediate points, were selected to be analyzed further. The cases that present the best opportunity for comparison will be discussed in Section 4.5.

4.3 Experimental Setup

The addendum found in Appendix A, "Experimental Setup," can be referenced to see the overview of the entire setup. There were a few additions from the experimental setup described in Chapter 3 to accommodate the objectives for the experiment described in this chapter. This section will provide details pertaining to these additions, along with certain design choices not mentioned in the addendum.

Improvements From Pre-study

Similar to the pre-study, this experiment utilized high-speed imaging to capture the flame behavior after the electrical discharge ignited the gases. This experiment, however, had the additional objective of using a higher framerate to analyze the timescale of the ignition event. This additional requirement did not necessitate any alterations to the experimental setup.

Laser Diagnostics

As mentioned in Section 1.2, laser diagnostics were to be used in this experiment to analyze the flame chemistry of the various flames. To do this, OH Planar Laser-Induced Fluorescence (OH-PLIF) was used. This was done largely in part by Julia Lövgren, and detailed information regarding the background and experimental setup can be found in her report, [5]. The following figure shows a basic schematic of the concept of OH-PLIF as it was utilized in this experiment.

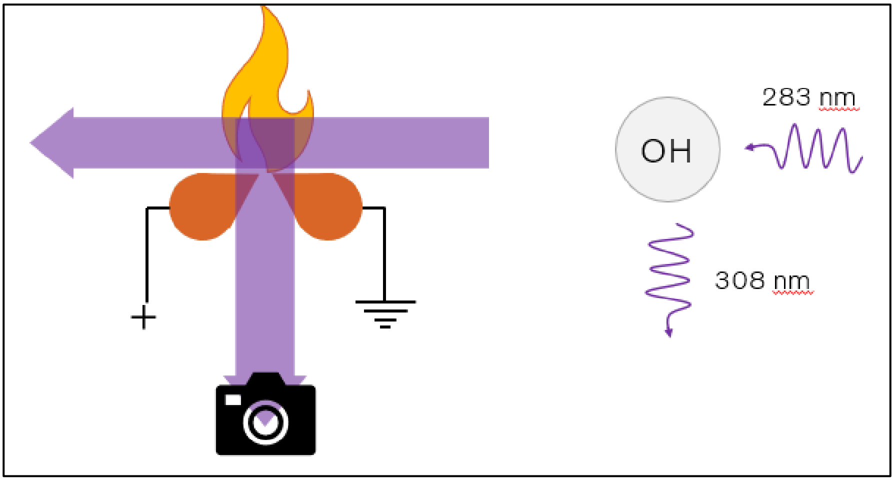

Figure 4.3: Schematic of OH-PLIF configuration [5]

The electrodes in the above figure, shown in orange, can also be seen in Figure 3.7. Changing the orientation and angle of these electrodes from the pre-study orientation (seen in Figure 2.3) was an important change to the setup as this provided maximum optical access for the laser diagnostics. The laser sheet, detailed in [5] would be blocked by the electrode tips, resulting in a smaller window of OH analysis.

4.4 Results and Discussion

This section is divided into two subsections. First, the results of the high-speed imaging of the ignition event at 150 kHz will be presented and discussed. Next, the high-speed imaging of the flame behavior at 10 kHz can be seen. Analysis of the flame behavior will incorporate results from [5] and ChemKin simulation results.

High-Speed Imaging – Ignition Event

The high-speed images were acquired at 150 kHz to investigate how the electrical discharge interacts with different gases to ignite them. Due to the expected very strong luminosity from the electrical discharge, the high-speed camera (Photron FASTCAM SA5) was employed without an intensifier. At this 150 kHz sampling rate, the camera setting was limited with short exposure time (6.42 microseconds) and low resolution (256 x144 pixel ratio). The combination of the high luminosity of the discharge and the low luminosity of the flame presents a few difficulties that will be mentioned in the following section.

Time Scale of Ignition Event

This section uses the high-speed images captured at 150kHz to depict the timescale of the ignition event as a result of the electrical discharge across a number of varying parameters. The results in Figure 4.4 show single-shot images of the initial discharge through the flowing gas medium over a time sequence of 73μsec. Table 4.1 describes the gas flow conditions of each image shown. At t=0, the gas is flowing, and the electrical discharge has not occurred yet. At this point, the capacitor bank is being charged until the voltage reaches the minimum breakdown voltage required to trigger an electron avalanche. As can be seen in Figure 4.4 below, the time between each single-shot image is 6.67 μsec, the fastest possible temporal resolution at 150kHz.

The frames in Figure 4.4 were selected in a way to show one frame in which there is no luminosity at all, indicating the discharge has yet to occur. The subsequent frame generally shows a slight glow coming from the electrodes. A total of 12 frames are included for each sequence to depict the dissipation of the flame kernel for each of the different cases. The combination of all of these cases together is intended to prove to the reader that the behavior of the ignition event varies from case to case. The effect of each changing parameter will be analyzed separately in the following sections.

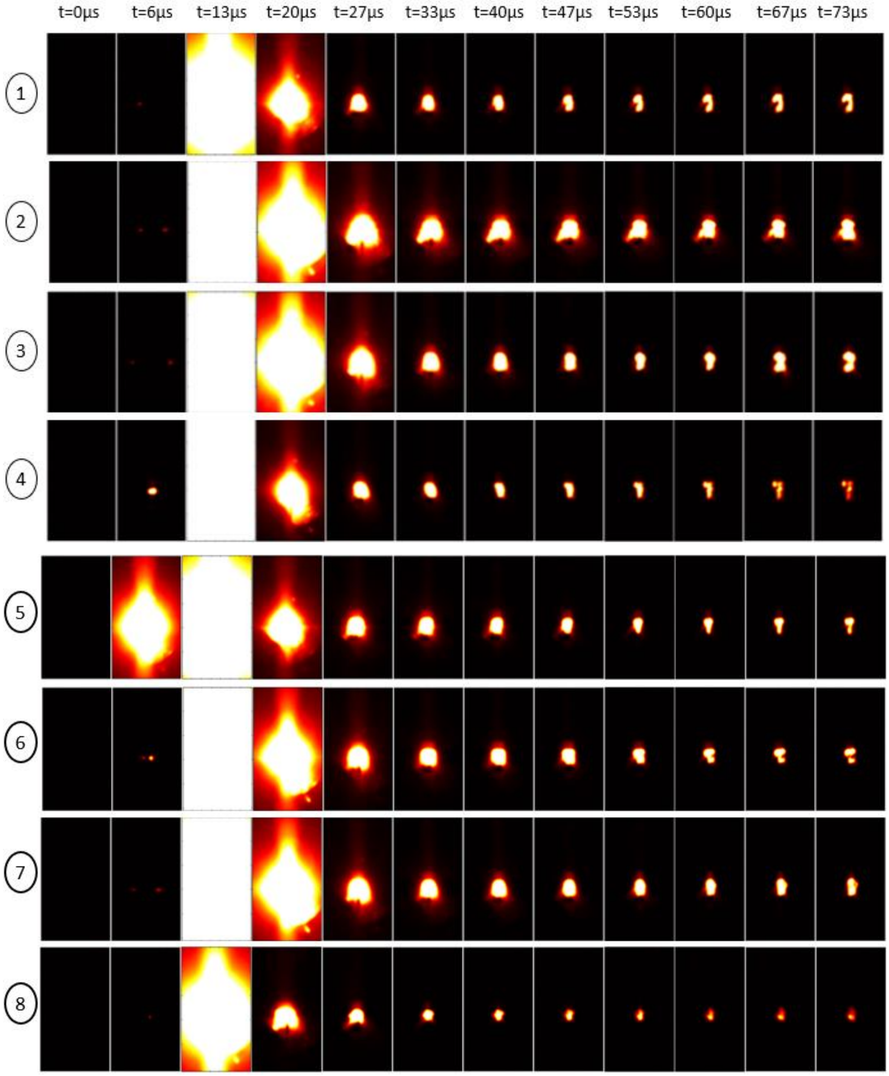

Figure 4.4: 150kHz sequence image of ignition event

Image No.	Gas	Gas Temperature (°C)	Flow Rate (m/s)	Equivalence Ratio
1	NCA	150	5	1
2	NCA	300	5	1
3	NCA	300	5	1.7
4	NCA	300	5	3.5
5	LFP	150	5	1
6	LFP	300	10	1
7	LFP	300	15	1
8	LFP	300	5	1.7

Table 4.1: Timescale of ignition, flow conditions

General Observations

For most of the cases seen in Figure 4.4, the starting of the ignition event triggered by the electrical discharge was observed in a single frame, presented here in the 3rd frame, where the signal intensity was saturated. For the fifth image, where the fuel was low explosive and the flow rate was 5m/s, the ignition event progresses slowly and therefore one intermediate step of the ignition process was captured, shown in the second frame. This implies the sampling rate of the imaging system was not fast enough to temporally resolve the initiation and evolution of the ignition process and therefore, the initiation and evolution process was discretely observed only in one frame. It is recommended for further investigation that a camera capable of capturing images at higher framerates, likely in the nanosecond scale, be implemented.

The captured frames are heavily dominated by the luminosity of the electrical discharge, and the actual flame is quite difficult to analyze. In all cases, the flame kernel was observed to be shrinking in size and intensity over time. Of course, the rate at which this occurred varied from case to case. This phenomenon will be described in the following sections.

Combining Time Scales

It can be seen quite clearly in Figure 4.4 that the discharge is occurring in the third frame and begins to dissipate in the fourth frame. This is considered to be the ignition event. There are also obvious differences in intensity and size in each different case shown. However, it is difficult to distinguish between the luminosity of the discharge and the luminosity of the flame kernel. In Figure 4.5, each image represents every 10th frame recorded (66.7 μs between images). Here, it is much easier to see the flame kernel separately from the discharge, but the discharge event itself cannot be seen. To gain an understanding of the entire event, it is best to analyze the behavior and characteristics of both the discharge and the flame kernel.

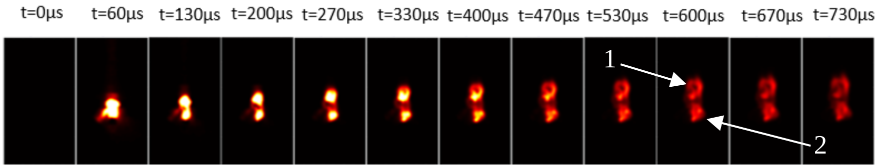

Figure 4.5: Sample ignition event at 66.7 μs temporal resolution

It is also important to note that due to the orientation and rigidity of the electrode setup, it can be confidently asserted that the electrical discharge does not move in the vertical direction. A gliding arc, for example, would show the discharge moving along the path of the electrodes, or changing in position vertically. As this is spark discharge, the discharge occurs strictly in between the two electrodes. Therefore, it can be surmised that the portion of luminosity propagating upwards in Figure 4.5 is the flame kernel. In the figure above, the portion labeled '1' denotes the flame kernel, while the portion labeled '2' is likely the intense luminosity of the discharge fading away.

In order to provide a better visual interpretation of the entire event, the two different time scales shown in Figure 4.4 and 4.5 will be combined into one image. These images will be used throughout the remainder of the analysis of the ignition event, using the same format. Take note of the time noted at the top of each image, so as to not be misled regarding the duration of the event. A sample of this combined image can be found below, with 'Set 1' denoting the set of images with 6μs between images, and 'Set 2' with 66 μs between images.

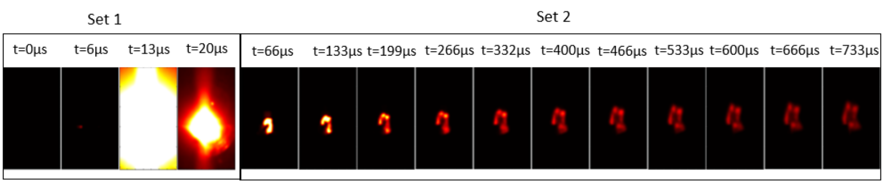

Figure 4.6: Sample image showing discharge and flame kernel behavior

Effect of Equivalence Ratio

In order to compare the ignition events of different equivalence ratios, we will take a closer look at three of the test cases found in Figure 4.7. These three cases can be shown below, and their flow conditions can be found in Table 4.2.

Image No.	Gas	Gas Temperature (°C)	Flow Rate (m/s)	Equivalence Ratio
1	NCA	300	5	1
2	NCA	300	5	1.7
3	NCA	300	5	3.5

Table 4.2: Flow conditions for Equivalence Ratio comparisons

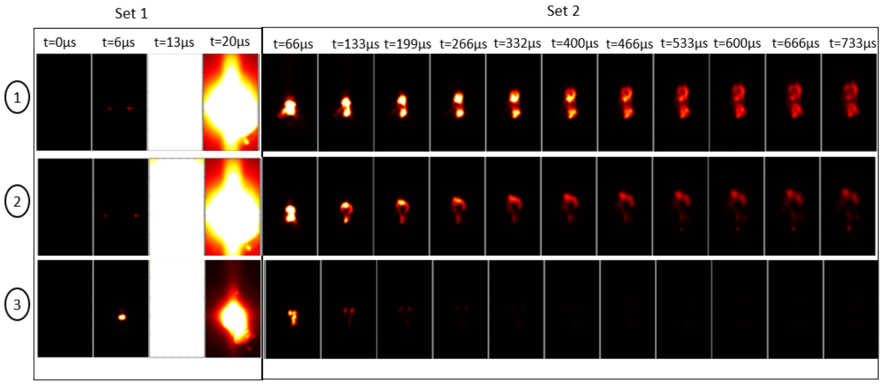

Figure 4.7: Ignition event for equivalence ratio comparisons

In Figure 4.7, it can be seen that the duration of both the flame kernel and the luminosity of the discharge dissipate quicker as the equivalence ratio increases. Image 1 represents the stoichiometric condition, with an equivalence ratio of 1, and has the highest intensity for the longest. At $\Phi = 3.5$, shown in image 3, the intensity of any luminosity dissipates very quickly. This can be attributed to two main factors, both of which stem from the increasing equivalence ratio.

As the equivalence ratio increases, the amount of fuel in the fuel-air mixture becomes more dominant. The length of the quartz mixing tube and the gas flow velocity both stay constant, implying the amount of time these gases have to mix is consistent between cases. The degree of mixing heavily impacts a mixture's ability to be ignited, as well as the resulting flame intensity. While it cannot be determined for certain the degree to which the gases are mixed (pre-mixed, partially pre-mixed or otherwise), comparatively it can be confidently concluded that the level of pre-mixing is highest with most intense flame kernel (image 1) and lowest with the quickly dissipating flame kernel (image 3).

Additionally, the flammability limit has a profound effect on flame intensity, and subsequently, the intensity of the flame kernel shown in these images. Referring back to Figure 4.2 (NCA scan), it can be seen that the equivalence ratio was not increased enough to determine the upper flame limit for this gas mixture. However, it can clearly be seen that with increasing equivalence ratio, the fuel-rich mixture struggles to maintain any intensity in both the discharge and the flame kernel.

It is also interesting to note that in set 1 showing the smaller time scale of images for image 3, more intensity can be seen at the electrodes in frame 2 in comparison to the lower equivalence ratios. However, due to the discharge event taking place on a timescale in the order of nanoseconds, it is not possible to draw conclusions as to the reason this is the case.

Effect of Temperature

To gain some insight into the impact gas temperature has on the ignition event, we will take a closer look at two of the test cases found in Figure 4.8. These two cases can be shown below, and their flow conditions can be found in Table 4.3.

Image No.	Gas	Gas Temperature (°C)	Flow Rate (m/s)	Equivalence Ratio
1	NCA	150	5	1
2	NCA	300	5	1

Table 4.3: Flow conditions for temperature comparisons

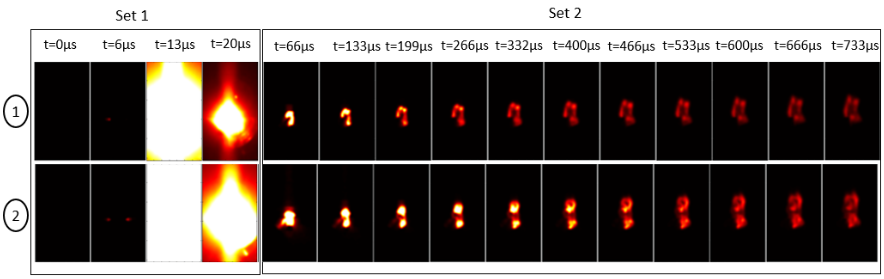

Figure 4.8: Ignition event for temperature comparisons

When the gas temperature is higher, as seen in image 2, the intensity of both the flame kernel and the discharge are sustained longer. This is to be expected, as the increased temperature indicates increased energy input. It can also be seen that the flame kernel at the higher temperature propagates upwards away from the discharge at higher speed. This can be attributed to two main factors: increased reaction rate, and increased flame speed.

As the gas temperature increases, the rate at which the reactions of the combustion process occur increases. The higher energy coming from the higher temperature promotes the activation of the chemical reactions, leading to a more rapid release of heat and subsequently a higher flame kernel intensity.

The laminar flame speed of a gas increases with gas temperature. As the laminar flame speed increases, the rate at which the flame kernel propagates will also increase. For this reason, there is a visible separation between the luminosity of the discharge and the flame kernel in the higher temperature gas (image 2). Laminar flame speed will be discussed further in the Flame Behavior section.

Effect of Flow Rate

To identify the impact gas flow velocity has on the ignition event, we will take a closer look at three of the test cases found in Figure 4.9, and their flow conditions can be found in Table 4.4.

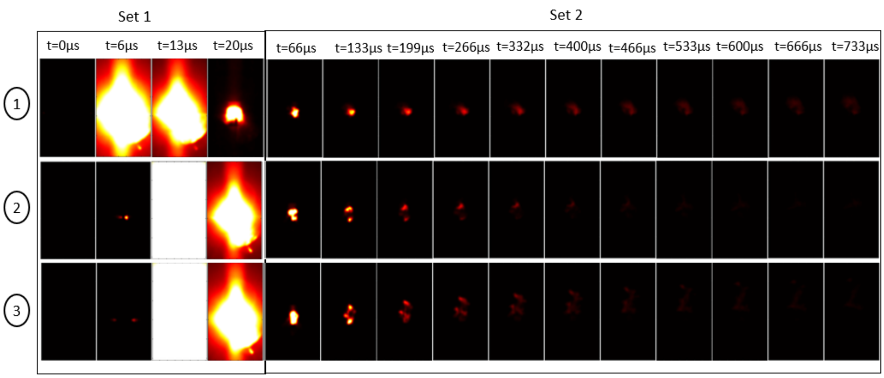

Figure 4.9: Ignition event for gas flow velocity comparisons

Image No.	Gas	Gas Temperature (°C)	Flow Rate (m/s)	Equivalence Ratio
1	LFP	300	5	1
2	LFP	300	10	1
3	LFP	300	15	1

Table 4.4: Flow conditions for gas flow velocity comparisons

As was mentioned in the previous section, the degree to which these gases is mixed has a significant impact on the combustion. Increasing the flow rate will decrease the residence time, meaning they have less time in the quartz tube to mix. In Figure 4.9, image 1 has the lowest flow velocity, and therefore the highest residence time. This is supported by the fact that the duration of the intensity is the longest for this case, and shortest in the high velocity (15 m/s) case shown in image 3. For all cases, the intensity diminishes within a few frames. This can be attributed to the fact that the LFP gas mixture is less reactive, as it is dominated by CO_2.

Effect of Gas Composition

Obviously, the gas composition of a mixture will have the most outright impact on behavior in an ignition event. The chemical makeup of a gas will dictate all reactions, while temperature and flow rate may affect the rate and extent to which these reactions occur. For this reason, it is extremely important to understand how different gas compositions behave at the point of ignition. To do this, the following cases have been chosen. As can be seen in the Table 4.5, the flow rate, temperature and equivalence ratios are all the same between the two cases.

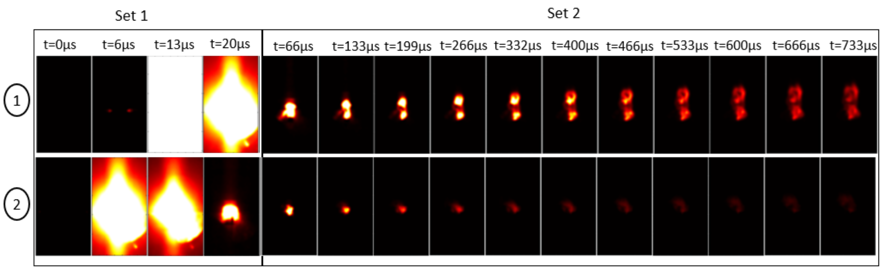

Figure 4.10: Ignition event for gas flow velocity comparisons

Image No.	Gas	Gas Temperature (°C)	Flow Rate (m/s)	Equivalence Ratio
1	NCA	300	5	1
2	LFP	300	5	1

Table 4.5: Flow conditions for gas flow velocity comparisons

In Figure 4.10, it can immediately be seen that the overall intensity shown in the frames is much higher and much more sustained in the NCA gas mixture (image 1) than in the LFP gas mixture (image 2). Referring back to Table 2.1, which breaks down the gas composition of each mixture, it can be seen that the NCA gas mixture is comprised of 42.8 % H_2 and 10% CO_2, whereas the LFP mixture has 29.5% H_2 and 48.4% CO_2. Because CO_2 is chemically inert, it does not readily react with other substances. The high concentration of CO_2 in the LFP gas compared to the NCA, in combination with the high level of H_2 in the NCA gas, makes NCA a much more reactive mixture.

High-Speed Imaging – Flame Behavior

The data presented in this section was collected at 10kHz with a shutter speed of 99.75 microseconds. Due to the slower shutter speed and longer exposure time, collecting data at this framerate made it possible to focus on the behavior of the flame as several variables change. Unless it is specifically stated otherwise, the images shown were recorded AFTER the ignition and turning off the discharge. In other words, the flame had already been ignited at the point the recording started.

Each subsection shows a series of sequence images, and an average flame image. The average flame image shows the average flame intensity over the time span of which the sequence image was taken.

Effect of Temperature

The cases chosen to depict the impact of gas temperature on flame behavior can be seen in Table 4.6. There are two sets of similar flow scenarios, where the only variable changing is the gas temperature. While the impact of gas composition will be analyzed in a separate section, it is important to identify how a specific variable's impact on flame behavior changes for different gases. In other words, the magnitude to which increasing the temperature changes the flame's behavior for one gas might be very small, while changing the gas temperature for another gas may have an enormous impact on flame behavior. For this reason, data was collected to show the temperature's impact on flame behavior for both the NCA and LFP gas mixtures.

Image No.	Gas	Gas Temperature (°C)	Flow Rate (m/s)	Equivalence Ratio
1	NCA	150	5	1
2	NCA	300	5	1
3	LFP	150	5	1
4	LFP	300	5	1

Table 4.6: Flow conditions for temperature effect comparisons

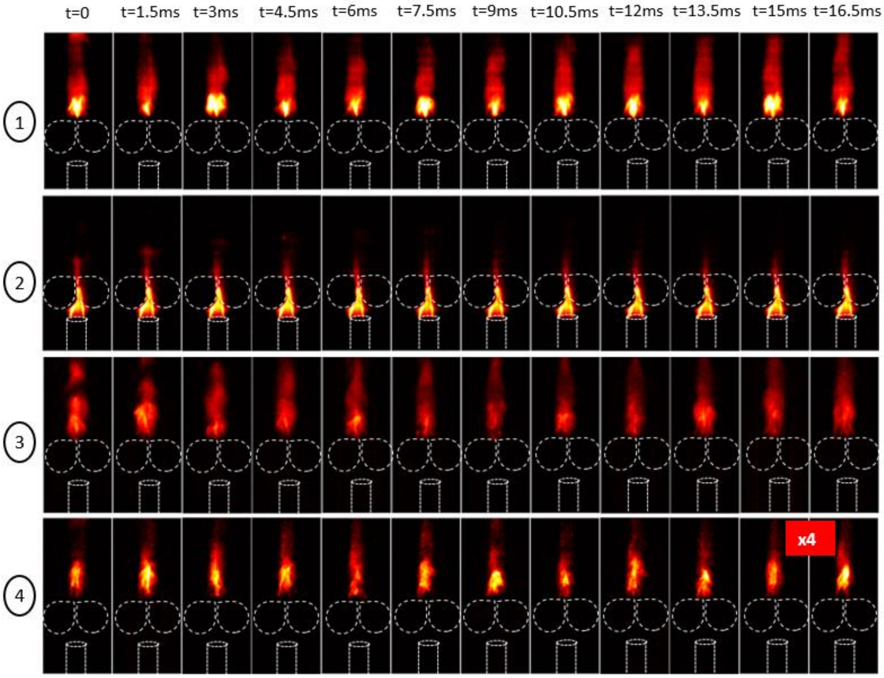

Figure 4.11: Sequence images of equivalence ratio comparisons over a time span of 16.5ms

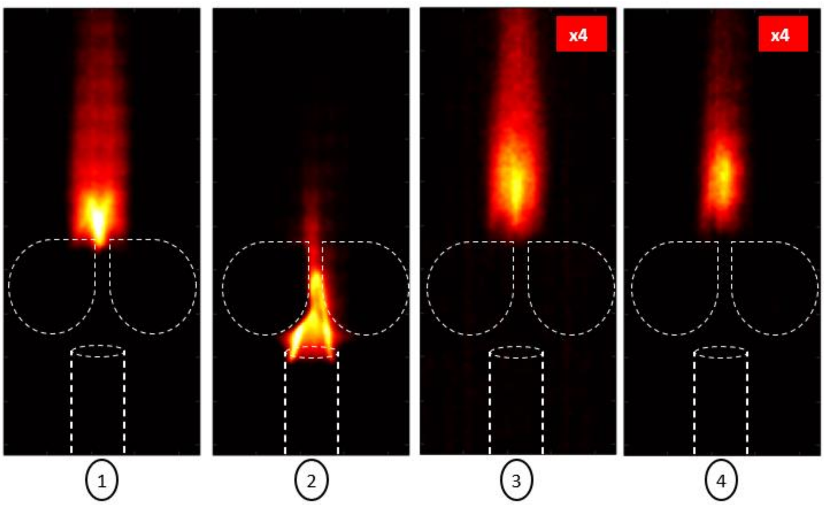

Figure 4.12: Average flame image of equivalence ratio comparisons over a time span of 16.5ms

With an increase in temperature, the flame intensity and laminar flame speed increases. This can be seen immediately in Figure 4.12 when comparing the NCA gas mixture at 150 °C (image 1) and 300 °C (image 2), as the flame changes from being anchored at the electrodes to being anchored at the mixing tube. The flame also becomes more compact and centralized at higher temperatures. For the LFP gas mixture (images 3 and 4), the impact of preheating is not quite as significant.

Effect of Equivalence Ratio

To determine how the fuel-air ratio impacts the flame behavior, the cases in the following figure were analyzed. Using the high explosive gas mixture at 300C and a constant flow rate of 5 m/s, the amount of air mixed with the fuel was varied. Table 4.7 depicts the flow conditions of the gas mixture, showing the increasing equivalence ratio of the different test cases.

Image No.	Gas	Gas Temperature (°C)	Flow Rate (m/s)	Equivalence Ratio
1	NCA	300	5	0.8
2	NCA	300	5	1
3	NCA	300	5	1.7
4	NCA	300	5	3.5

Table 4.7: Flow conditions for equivalence ratio comparisons

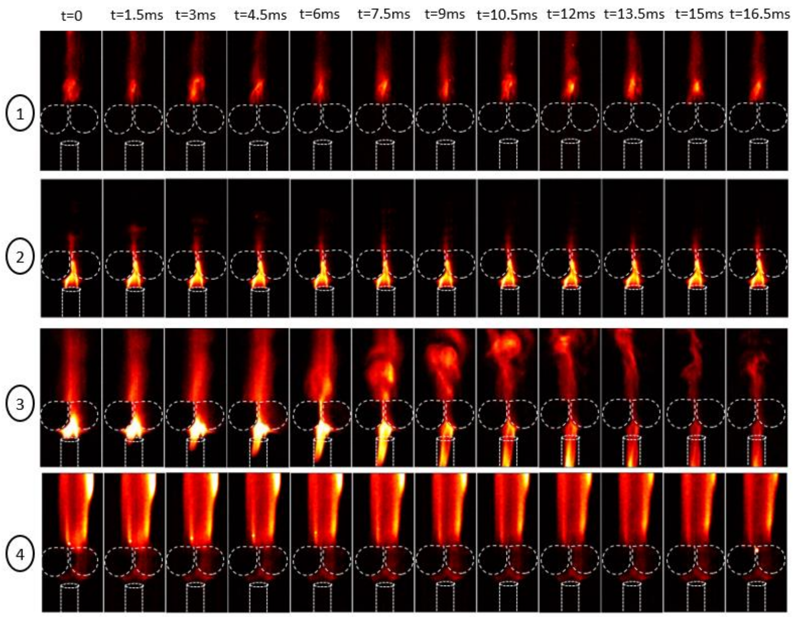

Figure 4.13: Sequence images of equivalence ratio comparisons over a time span of 16.5ms

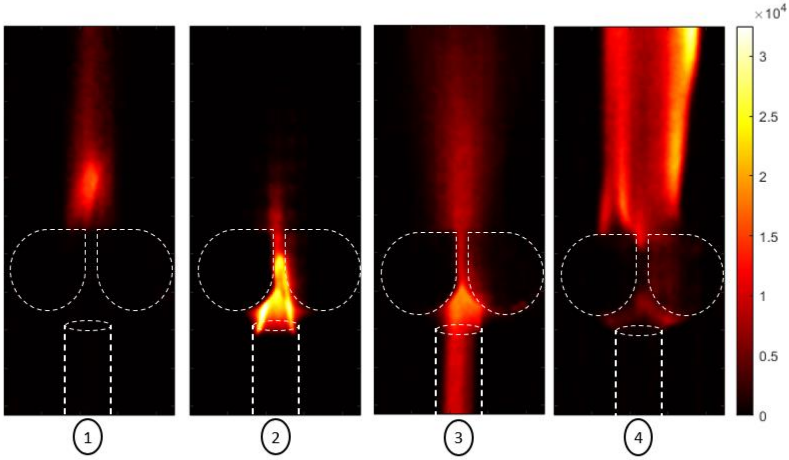

Figure 4.14: Average flame image of equivalence ratio comparisons over a time span of 16.5ms

Flame Anchoring Location

Figures 4.13 and 4.14 demonstrate several different behaviors that are a result of a number of different factors. At the lowest equivalence ratio shown, Φ = 0.8, the flame is anchored at the electrodes downstream of the mixing tube. At Φ = 1, shown in image 2, the flame is anchored at the outlet of the mixing tube. When the equivalence ratio is increased to 1.7, the flame propagates downstream for a duration of about 3 ms, then begins to propagate upstream, back into the mixing tube. This behavior is known as flashback. At the highest equivalence ratio shown, Φ = 3.5 (image 4), the flame returns to being anchored on the mixing tube.

These different anchoring behaviors can be largely attributed to the laminar flame speed of the NCA gas mixture. Figure 4.15 shows a graph of laminar flame speed plotted against equivalence ratio for both the NCA and LFP gas mixtures. This was created using the chemical kinetics modeling software ChemKin. The points on the plot correspond to the equivalence ratio and laminar flame speeds of the images presented in Figures 4.13 and 4.14.

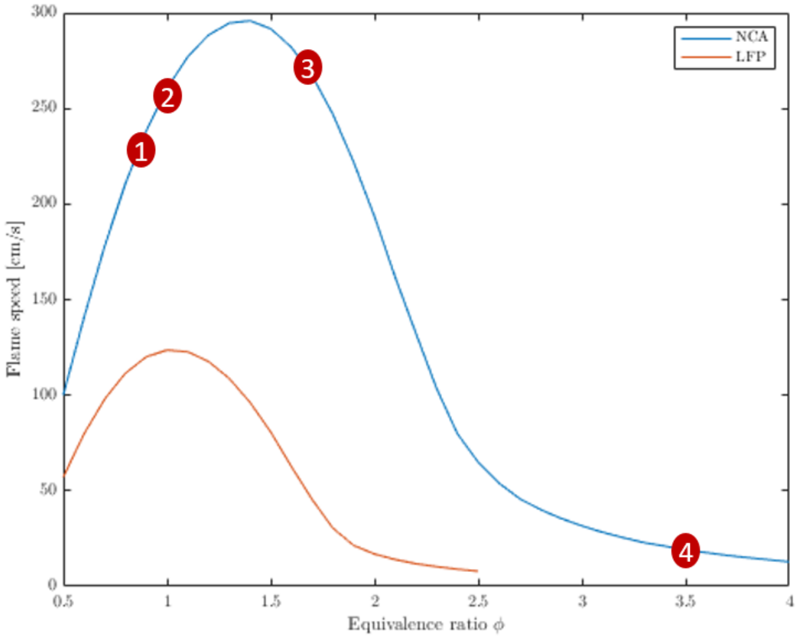

Figure 4.15: Laminar flame speed vs equivalence ratio

The point at which each flame is anchored can be directly linked to each case's laminar flame speed. At the point of ignition, the flame propagates in all directions at this given flame speed. Meanwhile, the gas flow velocity is flowing out of the tube, countering the downward propagation of the flame. Case 3, for example, has the highest flame speed. As it can be seen in image 3 in Figure 4.13, the flame propagates upstream back into the tube, implying that the laminar flame speed was sufficient to overcome the opposing flow exiting the tube.

Case 2, which has the second highest flame speed of the cases shown, anchored on the quartz tube. This means that the laminar flame speed was high enough to emit a sufficient amount of heat toward the exit of the mixing tube, but not high enough to completely overcome the gas flow and propagate upstream like case 3. As the heat in case 2 localized around the exit of the mixing tube, the point of ignition shifted from the initial point of ignition in between the electrodes down to the tube exit.

Case 4, when Φ = 3.5, does not exactly follow this trend. The flame is observed to be anchored at the exit of the mixing tube, and the flame is quite elongated. This can be attributed to the fact that under these conditions, the flame is sustained in a diffusion-like mode. The entrainment of air from the surroundings needs more time to blend with the heavy fuel-enriched mixture to dilute the gas mixture to an equivalence ratio below the upper flammability limit. Consequently, the flame demonstrates this elongated shape. This can be seen further in Figure 4.16, from [5]:

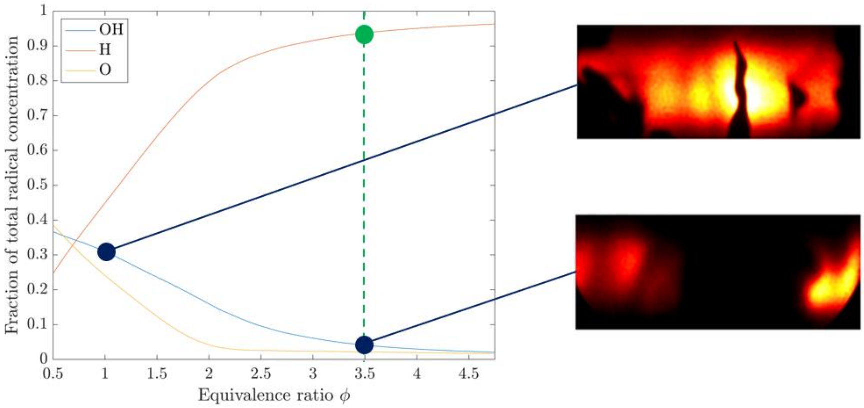

Figure 4.16: Radical concentration vs equivalence ratio [5]

The plot, also created in ChemKin, shows that as the equivalence ratio increases, the prevalence of the OH radicals decrease. The images included show the OH distribution, gathered by Julia Lövgren. Under fuel-rich conditions, the H radicals become increasingly prevalent, indicative of a diffusion flame.

This presents a crucial conclusion: The sustainability of a flame resulting from ignition of the NCA gas mixture is not driven by OH, but rather by H. This indicates the combustion process can occur and be sustained even where there is a low amount of oxygen present. This has major implications in the consideration of design and safety protocols for battery safety.

4.5 Conclusion and Future Outlook

This section will describe the possible areas of research that may increase understanding of the phenomena observed in this chapter.

Battery Safety

Battery safety is a critical aspect of the EV industry, and understanding the combustion behavior of potential battery vent gases is vital in improving safety. As it was mentioned in the previous section, the NCA gas mixture exhibited combustion behavior that was driven by H radicals rather than OH. This insinuates that the flame can be sustained with a low oxygen supply.

The current battery venting system designs are typically optimized for managing OH-driven combustion. Additionally, extinguishing methods of these battery fires typically depend on suffocating the flame, and depriving it of oxygen. Depending on the current battery venting system design, this can prove to be hazardous. It should be mentioned, however, that the radicals that drive the combustion of these vent gases are heavily dependent on the composition of the gases themselves. For this reason, further studies should be done on a wide range of possible vent gases to better understand the risk associated with this.

One approach to enhance battery safety is to investigate the composition of the vent gases under various conditions. The specific gases produced during battery venting are influenced by several factors including the battery chemistry, temperature, state of charge, and external factors like physical damage or thermal abuse. Therefore, conducting comprehensive studies on a wide range of possible vent gases becomes imperative to better comprehend the risks associated with different battery scenarios.

Ignition Event

The study of the physical spark discharge during battery venting in a thermal event is crucial in understanding the safety and behaviors of EV battery fires. It was determined that the high-speed imaging used to capture the discharge event was still too slow to fully understand the behavior of the physical spark discharge. Using a higher framerate to capture this behavior can provide some critical insight into the interaction of the electrical discharge and different battery vent gases. Consequently, it will aid in predicting potential hazards and designing venting systems that can handle a diverse range of scenarios. As mentioned, this report presented the ignition event recordings at 150kHz. It is likely that a camera will be required to have the capability of capturing the event in the nanosecond time scale.

5. References

[1] Warnatz, Jürgen & Maas, Ulrich & Dibble, Robert. (2006). Combustion: Physical and Chemical Fundamentals, Modeling and Simulation, Experiments, Pollutant Formation. 10.1007/978-3-540-45363-5.

[2] Wang, Q. *et al.* (2019) 'A review of lithium ion battery failure mechanisms and fire prevention strategies', *Progress in Energy and Combustion Science*, 73, pp. 95–131. doi:10.1016/j.pecs.2019.03.002.

[3] Nilsson, E.J. (2023) *Evaluation of combustion properties of vent gases from Li-ion batteries*. publication. Energy Storage Materials, pp. 1–14.

[4] Subash, A.A. (2023) *Arcing as the ignition source in malfunctioning batteries*. publication. Swedish Electromobility Centre, pp 1-12.

[5] Lövgren, J. (2023) *Discharge and Flame Chemistry in Lithium-Ion Battery Vent Gases - Investigations using Breakdown Experiments with Laser-Based Diagnostics*. thesis report. Lund University, Combustion Physics Department

[6] Bhatt, A. (no date) *How a Battery Works, science.org.au*. Available at: https://www.science.org.au/curious/technology-future/batteries.

[7] Wang, Q. *et al.* (2012) 'Thermal runaway caused fire and explosion of lithium ion battery', *ChemInform,* 43(24). doi:10.1002/chin.201224210.

[8] Zhang, Q.-K. *et al.* (2021) 'Thermally stable and nonflammable electrolytes for lithium metal batteries: Progress and perspectives', *Small Science*, 1(10), p. 2100058. doi:10.1002/smsc.202100058.

[9] Rajzer, J.P. and Rajzer, J.P. (1997) *Gas discharge physics*. Berlin: Springer.

[10] Lu, X. and Laroussi, M. (no date) ‘On atmospheric-pressure non-equilibrium plasma jets and plasma bullets’, *Plasma Sources Science and Technology*, pp. 1–18.

[11] Nakayama, Y. (2018) ‘Spark tracing and electric discharge’, *Handbook of Flow Visualization*, pp. 67–96. doi:10.1201/9780203752876-6.

[12] Ramkumar, M.C. *et al.* (2018) ‘Polymer coatings for biocompatibility and reduced nonspecific adsorption’, *Functionalised Cardiovascular Stents*, pp. 155–198. doi:10.1016/b978-0-08-100496-8.00009-3.

[13] Fridman, A. (no date) ‘Physics and applications of the gliding arc discharge’, *The 31st IEEE International Conference on Plasma Science, 2004. ICOPS 2004. IEEE Conference Record - Abstracts.* [Preprint]. doi:10.1109/plasma.2004.1340190.

[14] Ruys, A. (2019) ‘Alumina as an electrical insulator’, *Alumina Ceramics*, pp. 413–445. doi:10.1016/b978-0-08-102442-3.00013-0.

[15] Shohet, J.L. (2003) ‘Plasma Science and Engineering’, *Encyclopedia of Physical Science and Technology*, pp. 401–423. doi:10.1016/b0-12-227410-5/00584-6.

[16] Beroual, A. and Coulibaly, M.-L. (2016) ‘Experimental investigation of breakdown voltage of CO2, N2 and SF6 Gases, and CO2-SF6 and N2-SF6 mixtures under different voltage waveforms’, *2016 IEEE International Power Modulator and High Voltage Conference (IPMHVC)* [Preprint]. doi:10.1109/ipmhvc.2016.8012898.

[17] P. Osmokrovic, M. Stojkanovic, K. Stankovic, M. Vujisic and D. Kovacevic, "Synergistic effect of SF6 and N2 gas mixtures on the dynamics of electrical breakdown," in IEEE Transactions on Dielectrics and Electrical Insulation, vol. 19, no. 2, pp. 677-688, April 2012, doi: 10.1109/TDEI.2012.6180263.

[18] Keysight Technologies (2019) ‘Evaluating Oscilloscope Signal Integrity’, *White Paper Keysight Technologies*, pp. 1–18.

[19] Bai, X.-S. (2023) ‘Turbulent Combustion’. Lund: Sweden, 8 April.

[20] Glassman, I. (1987) ‘Diffusion flames’, *Combustion*, pp. 238–291. doi:10.1016/b978-0-12-285851-2.50014-4.

A. Appendix A – Experimental Setup

This addendum, authored by Alexander Petersson and Julia Lövgren, is intended to provide readers with a fundamental understanding of the experimental setup used in the Enoch Thulin laboratories to execute both experiments detailed within this thesis report. The information included provides a detailed description of the setup as it pertains to the primary equipment, i.e., gas supply, power supply, electrode setup and major monitoring equipment used. It is crucial to know that this addendum does not include precautions taken to mitigate hazards within the lab, such as grounding wiring or laser protection. For safety precaution information, please see Appendix B.

The experimental work done by Alexander Petersson and Julia Lövgren in the Spring of 2023 builds on a pre-study setup completed by Arman Ahamed Subash, funded by the Swedish Electromobility Centre as seen in [4].

Overall Setup

This addendum does not include the cameras used to record the high-speed imaging and the OH-PLIF data, nor does it include any information about the laser or the optics used to form the laser sheet for the laser diagnostics. As the specs and setup for these specific pieces of equipment are particular to the individual application for which they were used, the information can be found in the main body of the individual reports produced by Alexander Petersson and Julia Lövgren. The rendering below in Figure A.1 shows the overall experimental setup.

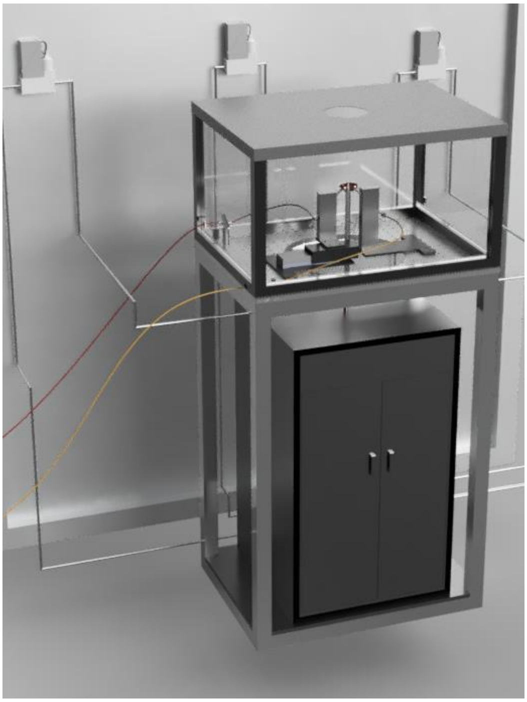

Figure A.1: 3D model of experimental setup in full

Electrode Setup

We begin with the two electrodes between which discharge occurs. Each one is made from a rod of stainless steel mounted on a Teflon piece and has a round copper head with a cone-shaped tip. The dimensions of the head given in millimeters are as shown in Figure A.2.

Figure A.2: Dimensions of a copper electrode head, shown in mm

The electrodes are mounted so that the upper edges are approximately horizontal, ensuring that the smallest distance between the electrodes is between the tips and that the view of the discharge channel between the tips is not blocked by the electrode heads when viewed from the side. The electrode serving as the cathode is connected to the output of a power supply, while the electrode serving as the anode is connected to the ground of the power supply. The power supply delivers between 0-15 kV and 0-100 mA. The cathode electrode position is fixed, while the anode is placed on a translational stage allowing the distance between the electrode tips to be changed. In between the electrodes, a quartz tube is placed with its opening positioned 2.5 cm below the tips of the electrodes. Through this quartz tube, the gas medium is supplied through which discharge occurs. A 3D rendering of the setup as seen from the side is shown in Figure A.3 below. It is important to note that Figure A.3 does not depict safety measures taken, including grounding wires, rubber sheets, screws, or specific fittings such as bolts and washers.

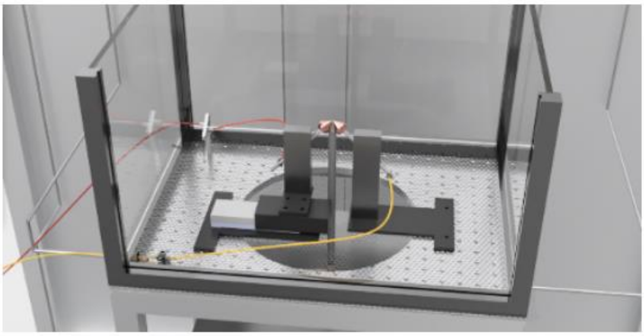

Figure A.3: 3D rendering of the electrode setup and wiring

Translational Electrode Stage for Cathode

One of the many significant requirements of the experiment detailed in Chapter 3 is the ability to horizontally translate one electrode with great precision. It was decided that one electrode, the anode, would remain stationary while the cathode would have the ability to move horizontally. In order to do this, the Thor Labs MTS25 motorized translational stage was implemented. In combination with the provided Thor Labs attachable stage, the electrode was able to be mounted on top of the translational platform and could be precisely moved. The motor was controlled through a wired connection which implemented a graphical user interface from APT Software.

Through this software, it was possible to move the electrode with precision in increments as small as 0.05 microns. In addition to providing the ability to move extremely small distances with great accuracy, the computerized control of the electrode minimized risk by eliminating the need to touch any equipment that had been exposed to dangerous amounts of electricity.

However, steps had to be taken to minimize the impact that the electromagnetic field from the high voltage would have on the functionality of this motor. To avoid any possible interference and minimize the amount of exposed metal near the electrodes, a 'shield' was modeled and 3D printed to fit around the motor. This can be seen in the previous image, Figure A.3. It was also covered with aluminum foil, and a non-conductive, heat-resistant material to provide further protection.

Gas Supply

The gas medium is supplied to the quartz premixing tube via a three-line configuration as shown in Figure A.4, where flammable gas, oxidizer and heated inert gas were supplied separately. The quartz tube has an inner diameter of 9 mm and a length of 20 cm, providing optical access and electrical insulation from the electrodes. As previously mentioned, the distance from the electrode tips to the outlet of the quartz tube was 2.5 cm, which is considered to minimize surrounding air entrainment while still not having the electrodes severely obstructing the flow.

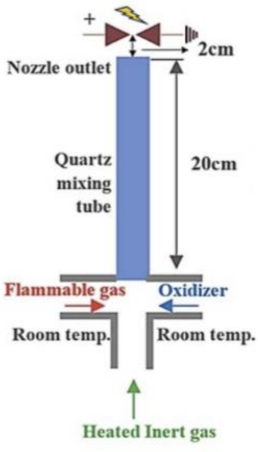

Figure A.4: Three-line gas flow configuration, schematic from [4]

The inert gas line passed through a furnace (Entech VSTF 50/11), providing the possibility of heating the inert gas. The flammable gas and oxidizer were injected as counterflows horizontally as shown in the sketch in Figure A.4, while the heated inert gas was injected vertically upwards through the quartz tube. The quartz tube is considered a preheat zone of the gas mixture resulting from the mixing of the three gases. The flammable gas and the oxidizer are at room temperature before mixing. The inert gas line and the oxidizer line are connected to the building's main gas supply lines, while the flammable gas line is connected to a high-pressure gas bottle. Upstream of the mixing point, each gas flows through a mass-flow controller (Bronkhorst El-Flow) allowing for precise volumetric flow rates to be specified. Upstream of each mass-flow controller, each line has a check valve preventing backflow toward the main gas supply or the high-pressure gas bottle. Additionally, there is a flame-quenching porous material at the base of the quartz tube to prevent excessive upstream propagation of the flame in the case of flashback.

Power Supply

The power supply consisted of two separate modules combining to deliver up to 16kV and 0-100mA. This power supply utilized a control module from Technix, designed to charge the capacitor bank and provide a front panel interface for controlling voltage and current settings. The capacitor bank used in this experiment was constructed in-house at the Enoch Thulin laboratories and has been used reliably within the combustion physics department at Lund University for a number of experiments. It is worth noting that this is the same power supply used in the pre-study [4], and therefore electrical inputs can be considered to be consistent in that aspect. Figure A.5 below is a photograph of the capacitor bank designed to provide the high voltage required to initiate an electrical discharge between the electrodes.

Current and Voltage Probes

A significant aspect of the experiment is the necessity to accurately measure the current and voltage at the point at which the electrical discharge occurs. For this, current and voltage probes were placed inside of the enclosed area and wired to an oscilloscope. Figure A.6 below shows the placement and wiring of the experimental setup when the probes were in use.

The oscilloscope used to measure the signals from the probes was a Teledyne

Lecroy Wavesurfer 3054Z, capable of 500MHz across 4 different channels. For this experiment,only2channelswereused.Inordertoprotecttheoscilloscopefromthe potentially damaging signal levels, 33 dB of attenuation was used on the channel measuring current. It is also important to note that the current probe output a signal of 1 volt per ampere measured.

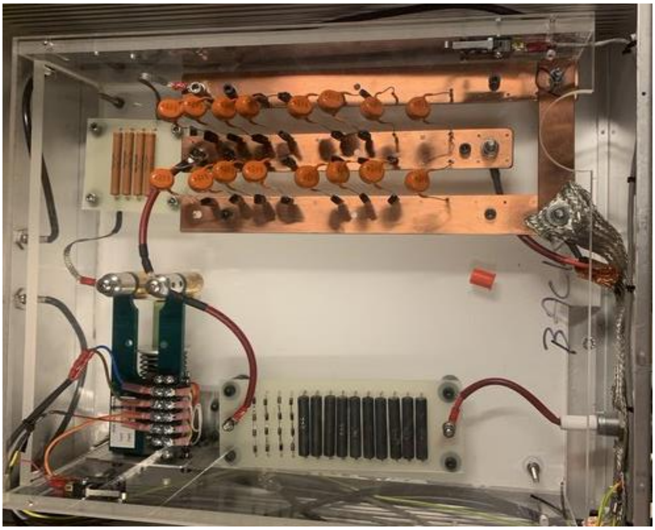

Figure A.5: Capacitor bank used for 16 kV power supply

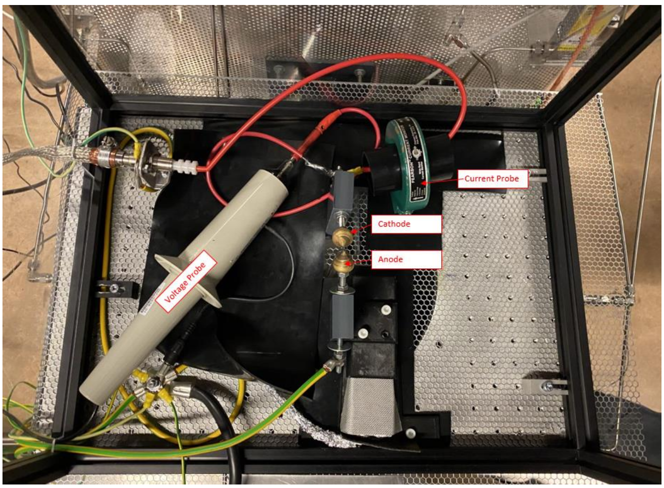

Figure A.6: Experimental setup with voltage and current probes viewed from above

B. Appendix B - Risk Assessment

The following document is a risk assessment of the setup described in Appendix A, authored by Julia Lövgren and Alexander Petersson.

Three main areas of risk have been identified. These are hazards regarding the electrical discharge and electrical circuits used to generate it, explosion and other risks related to gases, and hazards regarding the use of lasers for diagnostics. Measures to take in order to mitigate the risks related to these hazards are suggested here, as a complement to the working procedures in place at the Department of Combustion Physics, Lund University.

Electrical Hazards

- Short circuits can cause fires and electrical shock
- High voltage may cause shock
- Unintended sparks may ignite flammable material and gases
- Electricity used within EX zones has explosion risks
- The SS IEC Standard states that currents above 50 mA present a risk of potentially lethal heart fibrillation and burn injury. We work with 500A and high voltage power supply

In order to minimize electrical hazards and the risk of electrocution, steps have been taken to ground areas within the testing zone. Additionally, the following precautions should be taken to avoid adding unnecessary risk:

- Avoid extra materials within the testing area, such as liquids, books, pencils, etc. Any tools or equipment that may be needed within the test area should have non-conducting material for the handle.
- If inspection of the setup is needed, ensure power is disconnected.
- Keep electrical connections and switches clear. Ensure any new wiring can accommodate active current before addition to the setup.

Gas and Explosion Hazards

- The laboratory contains storage of combustible gases, permanent gas lines, fuel storage, ventilation and working benches where combustible gas is handled which are EX-classed as risk zones (for explosion hazards), thus posing a risk especially together with electronic equipment. Within these zones, ignition sources are not allowed, including electrical equipment.
- Handling of gas cylinders, regulators and piping.
- Health hazards related to gases include suffocation from low oxygen levels and poisoning from toxic gases. If the oxygen level in the breathing air (normally at 21%) is at 15%, you feel weak, at 13% you feel exhausted and at 10 % you have fainted.
- Flammable gases pose a risk of fire.
- Pressurized vessels of gas constitute an explosion risk.
- Condensed gases are kept at low temperatures, causing a risk of freezing injuries.
- Risk of gas lines not being resistant enough for their contents, or not suited for the pressure and temperature at which they are used.
- Power failure, causing ventilation loss. See above the risks regarding combustible and health hazardous gases.

The following precautions should be taken to avoid adding unnecessary risk:

- Due to the intentional ignition of combustible gases, flame containment is critical to avoid possible propagation of flame upstream toward the gas storage. A porous quenching mesh at the inlet of the mixing area provides one source of protection, while check valves in each flow line provide another.
- Become familiar with all sources of gas flow. Ensure flow is completely cut off when testing is completed, and there is no obstruction in any of the flow paths.
- Become familiar with fire extinguishers, including when and how to use. Ensure they are properly maintained and accessible. Restrict extra materials on top of testing “cage”, specifically flammable materials.
- Ensure the ventilation system is unobstructed and ready to be used.

- Flammable gases are to be kept in the specified area. Do not put any possible sources of ignition in or around this area and ensure proper maintenance of gas containers (no leaks or dents) and gas lines.

Hazards when Using Lasers

- Harm to eyes and skin
- Class 3B lasers may cause harm to the eyes and minor skin injuries, while class 4 lasers are harmful to the eyes both by direct viewing and by viewing of diffuse reflections from surfaces. Class 4 lasers are also harmful to the skin.
- Both class 3B and class 4 lasers pose a risk of fire.
- Damage to the skin may consist of both burn wounds (thermal damage) and photochemical damage, as well as skin cancer from repeated exposure.
- Injuries from lasers depend on both the dose of radiation and on the wavelength.
- The blink reflex of the eyes may protect the eyes to some extent from visible light. Extra caution is needed when using ultraviolet lasers since they do not trigger the reflex.

The following precautions should be taken to avoid adding unnecessary risk:

- Use appropriate eye protection when lasers are in use if necessary. Laser operation in this laboratory should be able to be performed without being in the area of the laser, so avoiding the area during laser use altogether would minimize risk.
- Ensure the testing area is clear of extra materials that may interfere with laser diagnostics, can diffuse or reflect lasers, or be damaged by lasers.
- Become familiar with the control of the laser system. If applicable, understand when and how to use a disconnect switch to manually deactivate the laser.
- To minimize risk in all areas mentioned in this document, unauthorized persons should not be permitted in the lab during operation.